2015

FINITE ELEMENT ANALYSIS OF A HYDRAULIC SNUBBER WITH RESPECT TO HISTORICAL TEST DATA AND AMERICAN SOCIETY OF MECHANICAL ENGINEERS REQUIREMENTS

Matt Palmer
University of Rhode Island, mattpalms@yahoo.com

FINITE ELEMENT ANALYSIS OF A HYDRAULIC SNUBBER WITH RESPECT TO HISTORICAL TEST DATA AND AMERICAN SOCIETY OF MECHANICAL ENGINEERS REQUIREMENTS

BY

MATT PALMER

A THESIS SUBMITTED IN PARTIAL FULFILLMENT OF THE

REQUIREMENTS FOR THE DEGREE OF

MASTERS OF SCIENCE

IN

MECHANICAL ENGINEERING AND SOLID MECHANICS

UNIVERSITY OF RHODE ISLAND

2015

MASTER OF SCIENCE IN MECHANICAL ENGIENERING

OF

MATT PALMER

APPROVED:

Thesis Committee:

Major Professor David Taggart

Bahram Nassersharif

Fred Vetter

Nasser H. Zawia
DEAN OF THE GRADUATE SCHOOL

UNIVERSITY OF RHODE ISLAND
2015

ABSTRACT

Hydraulic snubbers are either acceleration or velocity limiting seismic restraints designed to restrict movement of piping or equipment during dynamic events or operational transients. In a piping analysis, snubbers are modeled as linear elastic spring elements governed by Hooke's law, F = kx. Snubbers are widely used in nuclear power plants, and as such their qualification testing to verify the spring constant k is governed by American Society of Mechanical Engineers (ASME) codes. ASME mandates experimental determination of spring constant k where practical, or a combination of testing and analysis when not practical. This qualification test includes testing at full load under a sinusoidal forcing function at a maximum frequency of 33 Hz.

There remains a practical upper limit to dynamic testing that is imposed by the availability of test equipment. This upper limit is governed by the size of the hydraulic pumps and servo actuators supplying fluid to the actuating test cylinder. At current writing, this limit is approximately 200 kips @ 33 Hz. New reactor designs have applications for snubbers with load capacities up to 1,900 kips. Functional testing can be conducted on these large units to verify the lockup and bleed parameters are correct, as well as the load carrying capacity. However, the dynamic spring rate of the snubber will not be experimentally verified at full rated load.

This study developed an FEA model of a hydraulic snubber that was compared to existing ASME qualification test data performed by Anvil Engineered Pipe Supports (EPS). If an accurate model can be developed for smaller snubber sizes, it

can be used to determine the spring rate of units that exceed the capacity of existing test equipment.

The experimental test data shows a spring constant that decreases at an approximately linear rate between 3 Hz and 33 Hz, with a reduction at higher frequencies of approximately 30%. The simulation models linear elastic behavior, and shows up to a 6% reduction between 3 Hz and 33 Hz. Part of the discrepancy can be explained by the load controlled nature of the test negating inertial effects, and increased deflections due to lost motion caused by assembly clearances and manufacturing tolerances. Further testing should be conducted, measuring load through pressure transducers in the cylinder fill ports to overcome these test setup limitations. This testing should be done on at reduced load so that a model can be developed that agrees with both the reduced load testing and rated/emergency load testing.

ACKNOWLEDGMENTS

I would like to acknowledge Professor David Taggart of URI for his assistance in writing this thesis, and being flexible in working with me.

I would also like to acknowledge Rick Richards of ITT Grinnell Corp and Anvil Engineered Pipe Supports, as this thesis builds on his 35 years of contributions to the nuclear power industry.

And to my wife, without whose support this paper would not be possible.

TABLE OF CONTENTS

LIST OF TABLES

LIST OF FIGURES

CHAPTER 1

Definition and Principles of Operation of Hydraulic Snubbers

A pipe support is an integral part of any nuclear power plant. Pipe supports are load bearing components that support the weight and guide the thermal growth of safety and non-safety related piping systems and equipment. Pipe supports consist of nearly infinite configurations, but all have the same recipe:

1) Structural Attachment – Typically consists of a bracket or lug welded to the building structural steel or bolted to the building foundation or containment structure
2) Pipe/Equipment attachment – A clamp designed to fit around a pipe or lug welded to equipment (pump, steam lines, pressurizer, etc)
3) The "middle" – The pipe support component that functions as required by analysis. Will allow thermal growth, apply a load to the system, or restrain pipe movement as needed.

Figure 1 shows typical pipe support assemblies on 34" hot reheat lines at a natural gas combined cycle power plant. When in operation, these lines will operate at a temperature of approximately 1050° F, causing several inches of thermal movement. Figure 2 is a typical snubber assembly per Figure NF-1132-1(c) [1]. There are many other types of pipe support components, but for the purposes of this paper, the discussion will be limited to shock and sway suppressors, also known as snubbers.

Figure 1 - Typical Pipe Support Assemblies at Sidi Krir Combined Cycle plant Alexandria, Egypt. Note the snubber in the background orthogonal to the run pipe. Palmer, Matt 2010

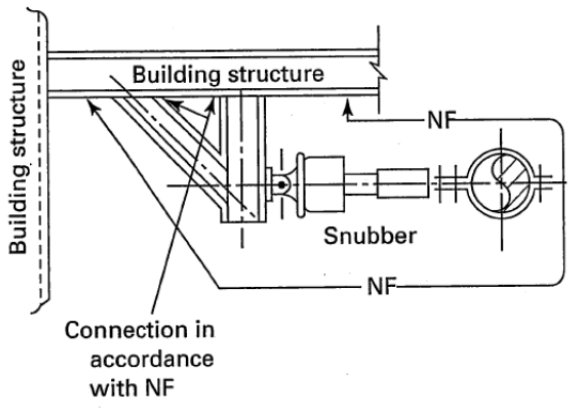

Figure 2 – Typical Snubber Assembly [1]

A snubber is a type of seismic restraint whose design was first conceived in the 1960's and began to see large scale use in the nuclear power industry in the 1970's [2, 3]. In a typical installation, it is attached to the building structure by a rear bracket and the piping system or equipment by a clamp, as in Figure 2. When the piping or equipment heats up during normal operation, a snubber is designed to allow thermal growth while applying minimal or no load to the system. It is operating in a passive mode. When subject to a velocity or acceleration greater than the pre-set limit, the restraint activates and applies resistance to any motion. Figure 3 shows a snubber installed on main steam piping at Diablo Canyon Nuclear Power Plant

Figure 3 – Snubber installation at Diablo Canyon Nuclear Power Plant. Kewalramani, Mohan "Support 414-414BSL". 2010

These passive and active modes of operation are common to the two types of snubbers present in industry today: Mechanical and hydraulic. Mechanical snubbers restrain motion through a ratcheting mechanism or an inertial mass limited to a pre-set angular acceleration. Hydraulic snubbers utilize valves to restrict the flow of fluid between the tension and compression sides of a hydraulic cylinder. Both mechanical and hydraulic snubbers can be velocity or acceleration limiting. This study is limited to velocity limiting hydraulic snubbers, specifically those manufactured by the Anvil Engineered Pipe Supports located in North Kingstown, RI (Formerly known as Grinnell Corp.).

Principles of Operation of Hydraulic Snubbers

Hydraulic snubbers are very similar in operation to any hydraulic actuator found commonly in industrial equipment, such as a forklift, hydraulic press, excavator etc… The primary difference is in the valve configuration. Where hydraulic actuators create motion of a piston rod by pumping fluid into either the tension or compression side of the cylinder, hydraulic snubbers resist motion by restricting fluid flow out of the tension or compression side. This fluid resistance through the valves prevents free movement of the piston, and a load is applied to the piping or equipment in the opposite direction of system motion. All snubbers are double acting, and will provide a resisting force in either tension or compression.

Functional Characteristics

Functional characteristics are so called because they can be field tested to verify that the snubber will perform its function as a dynamic restraint. The valve is a crucial component for the operability of a hydraulic snubber. On Anvil hydraulic snubbers, it consists of a check and bleed valve set in parallel on both the tension and compression sides. The check or lockup valve, is of the spring loaded poppet type. The bleed valve is a flow restrictor which provides resistance to flow as function of pressure. A typical control valve arrangement is shown in Figure 4.

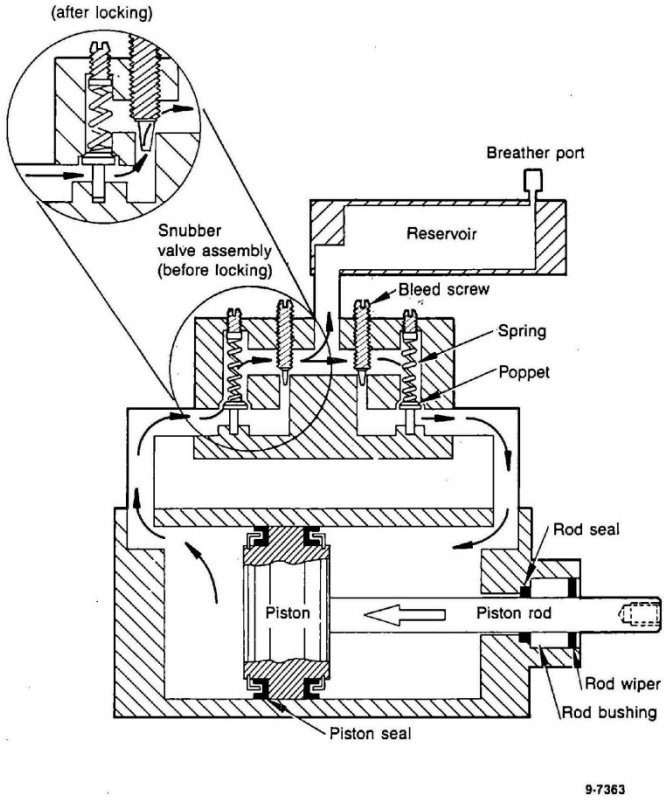

Figure 4 – Grinnell style control valve. [4]

In passive mode, the check valve is held open with a spring, and as fluid starts to flow over the poppet, a pressure differential develops between the reservoir and

cylinder side. As fluid flow velocity increases, the pressure difference becomes large enough to overcome the force of the spring holding the valve open. At this point, the snubber goes from passive to active, and the poppet closes. Fluid must now flow through the flow restrictor. Enough resistance is provided that the pressure inside the cylinder begins to increase, and a load is applied through the piston and piston rod.

A typical snubber pre-service test plot is shown in Figure 5. The test plot shows the two functional characteristics of a snubber that must be within specification to be installed in a nuclear power plant. These characteristics are defined in [5] as follows:

Activation – The change of condition from passive to active, in which the snubber resists rapid displacement of the attached pipe or component

Release Rate – The rate of the axial snubber movement under a specified load after activation of the snubber takes place

In the passive region, piston velocity is increased gradually. There is a minimal force required to move the snubber. This is referred to as drag. When the snubber piston velocity reaches the pre-set activation velocity, the fluid flow rate through the control valve is sufficient to close the poppet valve. In the test plot, this occurs at a piston rod velocity 8.2 inches per minute (IPM) in tension, and 9.6 IPM in compression. After activation, the load applied to the snubber piston rod is increased up to the load specified in the release rate, and the piston velocity is plotted as a function of load. In this case, the snubber has a release rate of 4.17 IPM in tension and 4.82 IPM in compression at a load of approximately 1500 lbf.

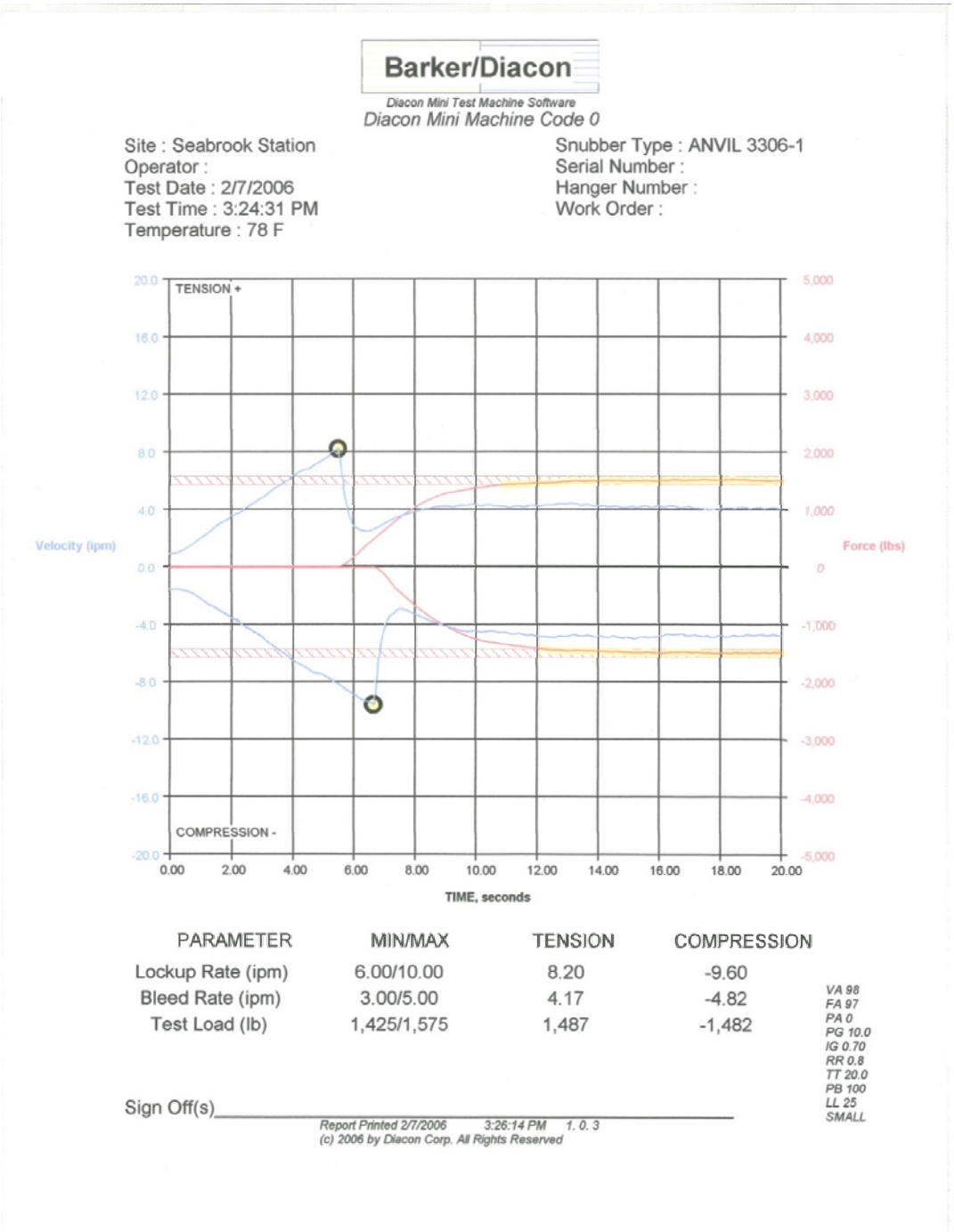

Figure 5 – Typical Pre-Service examination performed at Seabrook Station Nuclear Power Plant. Testing was performed on a Barker Diacon Model S2000 Test Bench with an Anvil Fig. 3306 Size 1 hydraulic snubber. Richards, Rick, 2006, Barker Diacon Fig. 3306 Functional Testing

A fundamental understanding of the functional characteristics of snubbers is required for interpretation of the dynamic test and simulation results discussed later. However, the activation velocity and release rate values have minimal effect on the dynamic performance of a hydraulic snubber. In the 1970's there was a large study done by the Grinnell Corporation on the effect of varying lockup and bleed velocities on dynamic spring rate [6]. It was determined that an upper limit of 40 IPM activation velocity and 25 IPM release rate would have negligible effect on the dynamic performance and operability of a snubber. Further discussion on the mechanisms of lockup and bleed are not relevant.

Drag force is defined in [5] as "The force that will sustain low-velocity snubber movement without activation throughout the working range of the snubber stroke". It is not of interest in most functional tests of hydraulic snubbers. Typical values for hydraulic snubbers are 2% or less of rated load. A snubber with a rated load of 10 kips should see a drag force of no more than 200 lbf. This resistance to motion is primarily caused by friction between the energized elastomeric seals and cylinder/piston rod. In most piping analysis, this drag force is neglected.

Dynamic Characteristics

Plant operations and maintenance personnel are concerned with the functional characteristics of a snubber; Plant design engineers are more concerned about the dynamic characteristics. These engineers analyze piping systems and equipment for their response to a ground excitation or operational transient, including water hammer, turbine trip, or pipe rupture. In their models, snubbers are placed at key node points to

restrain motion of the system and reduce piping stresses to within American Society of Mechanical Engineers (ASME) code allowables. To simplify analysis, an assumption is made that the seismic or transient velocities of piping and equipment are much greater than the pre-set activation velocity of a snubber. It can then be assumed that the snubber is a linear elastic spring element subject to Hooke's law, F = kx.

When subjected to a sinusoidal load, hydraulic snubbers exhibit a load/displacement relationship that follows a hysteresis loop, as shown in Figure 6.

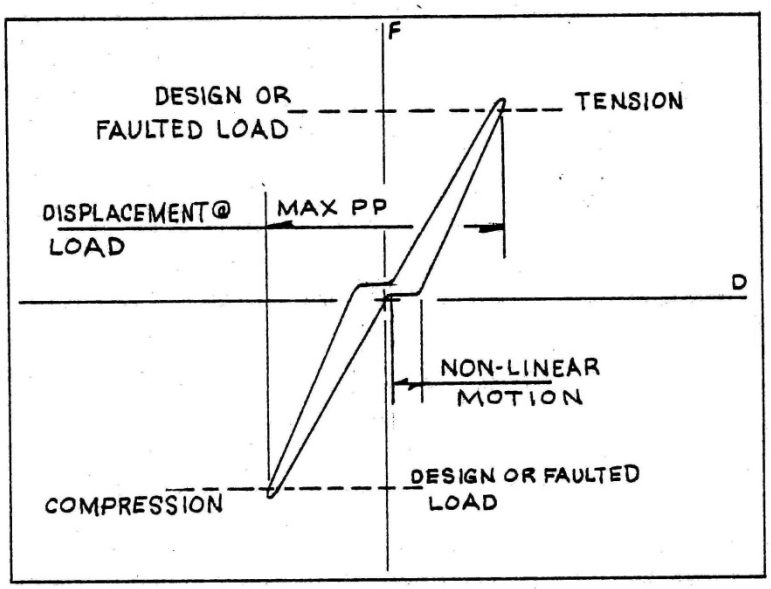

Figure 6 – Typical oscilloscope dynamic test plots [8]

From the plot in Fig. 6, the numerical value of k, or the dynamic spring rate of a snubber can be derived. The vertical axis represents load, and the horizontal axis displacement. The load and displacement of each cycle are plotted against one another, and the peak to peak loads and displacements are measured. Spring rate is defined in [9] as the "Applied load in tension and compression divided by the recorded

displacements in tension and compression". This corresponds to the equation $\frac{F_{max}-F_{min}}{\delta_{max}-\delta_{min}} = k$. The result k is usually given in units of kips/in.

The region of non-linear motion is known as "dead band". This is free-motion of the hydraulic snubber while activated with no resistance being applied to the piping or equipment. This is a consequence of clearances required for installation of load pins in the rod eye and pivot mount or mechanical gaps in the assembly due to manufacturing tolerances. At low frequencies (< 3 Hz), it is also includes the time required for the snubber poppet valve to close as the snubber cycles between tension and compression.

In practice, there are real limitations to the usefulness of the spring rate parameter of a hydraulic snubber. The two primary factors that contribute to a snubber's spring rate are the bulk modulus of the fluid and the position of the piston in the cylinder. Fluid bulk modulus can vary from batch to batch, as well as with temperature and pressure. For traditional hydraulic snubbers of a single piston rod configuration, the difference in fluid volumes of the tension and compression sides creates a different response for each position of piston travel. One can imagine the difficulties of accurately predicting the ambient temperature at each snubber location, as well as accurately modeling thermal movements to predict snubber piston position. The number of analysis load cases would grow exponentially.

To circumvent this complexity, the nuclear power industry wrote plant design specifications to include a Minimum Spring Rate parameter. In first generation design of large scale commercial reactors, overly conservative assumptions of accident conditions led to very stiff piping systems [12]. This then required manufacturers to

supply snubbers that will always be at least as stiff as the minimum spring rate value. This made analysis of large piping systems practical. For very critical equipment applications, such as steam generator, pressurizer, or reactor coolant pump snubbers, the engineer may specify a spring rate and require that the manufacturer test each production unit to verify the dynamic performance is within spec. This presents its own set of challenges and is the motivation for this study.

CHAPTER 2

History of Dynamic Qualification Testing and Development of ASME QME/QDR

Early snubber populations in the 1970's and early 1980's were prone to failure on a very large scale. Depending on the number of snubbers in service at each plant, failure rates hovered between 4% - 30% [2]. Fluid and seal compatibility issues with radiation and temperature caused many snubbers to leak or clog the valves, impairing their safety related function. Minimal or non-existent codes and requirements for snubber design qualification testing resulted in a low degree of confidence of their operability during a seismic event or transient. Compounding the problem is the fact that many early plant designs had upwards of 1000+ snubbers on their piping systems [2]. Optimizing seismic support locations in a piping analysis is an iterative process, and during the design phase of many plants, it was cheaper to buy more snubbers than it was to run hundreds of analysis iterations on mainframe computers. In some cases, entire plant populations were tested and/or replaced each refueling cycle at great expense in radiation exposure to plant workers, time and money.

The NRC began to address the issue of snubber operability as early as 1978, and incorporated it into its standard review of all licensee safety analysis by 1980 [11]. This put the onus on the licensee to provide proper assurance that safety related hydraulic snubbers would be operable during postulated seismic events or transients. Another consequence of the high failure rate of early snubbers was the development of

GE Specification 21A3502. This purchasing specification [13] addressed many deficiencies of hydraulic snubber design identified in the late 1960's and early 1970's, including environmental conditions, materials of construction, and dynamic performance. Many elements of this document made it into the Grinnell Corporation's design specification for hydraulic snubbers. By 1992, approximately 57% of all hydraulic snubbers installed in nuclear power plants were supplied by Grinnell [4]. As a result of this industry dominance, many of the design requirements from the GE specification became the accepted industry standard.

By the early 1980's, the issue of snubber operability had been solved from a regulatory standpoint [11]. Licensees began snubber reduction programs, more rigorous inspection regimens, and adoption of improved hydraulic snubber designs. However, it was also apparent that most licensees had two distinct snubber populations that required different approaches to qualification of the design and in-service inspection. Licensees and snubber vendors differentiated snubbers as large-bore and small-bore, sometimes also referred to as equipment and piping snubbers. The common definition of a large bore snubber is a snubber with a rated load of 50 kips or greater, and as of 1992, large bore snubbers made up approximately 10% of the US hydraulic snubber population [4].

A typical snubber maintenance plan for both large and small bore snubbers involves:

- Visual inspection of a pre-determined sample size

- Verification through testing of functional parameters of a pre-determined sample size. Figure 7 shows a typical hydraulic snubber test bench arrangement
- Verification of functional parameters of snubbers that fail visual inspection
- Expanded functional testing scope if a pre-determined number of functional test failures occur
- Repair or replacement of failed snubbers.

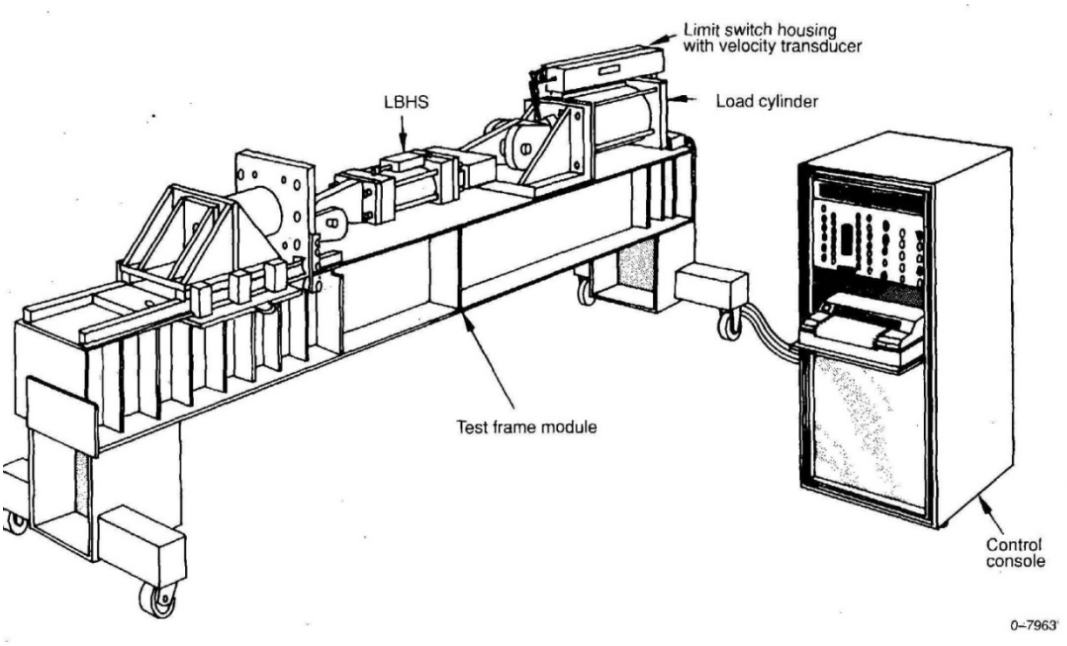

Figure 7 – Large bore hydraulic snubber (LBHS) in assembled in a functional test bench. [4]

In practice, functional testing and snubber repair/replacement activities involve removal of the snubber from service and installation onto a test bench. This can present real issues inside the containment structure, as space is limited and any time spent performing maintenance activities exposes plant personal to radiation. For small

bore piping snubbers, many designs are light enough that they can be carried by hand or maneuvered through tight spaces with minimal trouble.

Large bore equipment snubbers are much larger in size. Some cylinders have piston diameters as large as 20" and can weigh several thousand pounds. In many cases, it was deemed impractical to do any functional testing and prior to 1980, most large bore hydraulic snubbers were classified as inaccessible and were not subject to the same in-service functional testing of piping snubbers [4]. To rectify this, the NRC issued Generic Letters 80-99 and 84-13 [19, 20] requiring that all licensees add large bore hydraulic snubbers to their snubber surveillance populations. The first in-service functional tests of large bore hydraulics occurred at 13 plants between 1982-84. Each of these 13 plants had large equipment snubbers that failed to activate during testing, and would have been inoperable during a seismic event. In fact, all 14 steam generator snubbers at Palisades were found to be inoperable since initial reactor startup [10].

As a result of these serious safety deficiencies, the NRC created Generic Issue 113 which culminated in the technical evaluation NUREG/CR-5416, published in 1992 [4]. The technical evaluation determined that one of the main causes of large bore snubber failures was the lack of qualification testing for early designs. In many cases, design requirements for large bore snubbers were not properly specified by the licensee. Test equipment limitations in the 1960's and 1970's also prevented full scale static or dynamic testing of larger sizes. In fact, some designs did not see a proof-load test to verify that they were indeed capable of operating at full rated load. However, a survey of five large bore snubber manufacturers yielded that by 1992, qualification

tests that were very similar to the GE 21A3502 requirements had been conducted for many models with a rated loads of under 100 kips.

One of the recommendations made in NUREG/CR-5416 was to implement a uniform set of qualification standards for large bore hydraulic snubbers, either through a regulatory guide issued by the NRC or the addition of snubber qualification requirements to the existing ASME Qualification of Mechanical Equipment (QME) standard. ASME created a subgroup of the QME code to develop this standard. Given that the test requirements of GE 21A3502 had been adopted by several manufactures and were well understood by much of the industry, this specification became the basis for the development of the new testing standard. This standard became known as "Qualification of Active Mechanical Equipment Used in Nuclear Facilities Section Qualification of Dynamic Restraints", also known as QME/QDR [9]. QME-1-2007 was the first QME standard to be endorsed by the NRC for rulemaking in 2009 [14].

Current Snubber Qualification Testing

Nuclear power plants designed to ASME Section III 2007 or later must have their dynamic restraints qualified per ASME QME/QDR. The minimum requirements for functional and dynamic testing are outlined in in QME/QDR-6223.1 and presented in abbreviated form here

QDR-6223.1(a): Activation velocity or acceleration, as applicable, in both tension and compression

QDR-6223.1(b): Release rate in tension and compression at 5%, 10%, 25%, 50%, 100% of rated load and at a specified emergency load

QDR-6223.1(c): Initial force required to move the snubber in tension and compression (break-away drag, analogous to static friction)

QDR-6223.1(d): Drag force throughout the entire range of travel in tension and compression

QDR-6223.1(e): Measurement of Dead band

QDR-6223.1(g): The spring rate shall be tested by a dynamic cyclic loading equal to the rated load (or other specified load). The peak displacement range, including the dead band, shall be obtained during the dynamic cyclic test through the peak force range. The peak force range shall include load applied in opposite directions. Restraint movement shall be centered about the ¼, ½, and ¾ stroke locations according to the requirements of the functional specification. The testing frequency shall be from 3 Hz to 33 Hz at intervals of approximately 3 Hz. Each frequency shall last not less than 10 sec. Response at each frequency shall be recorded as load-displacement traces. No extreme change in displacement should be observed from one frequency to the next, as this could indicate that the fundamental frequency (natural frequency) resides in the 3 Hz - 33 Hz range.

QDR-6223.1(g) is written in its entirety here so the scope of dynamic tests involved in qualifying a hydraulic snubber is clear to the reader. Where testing is deemed unreasonable, qualification can be performed through dynamic testing at lower frequencies, drop testing, parent restraint qualification, analysis, or any combination thereof. The upper limit of 33 Hz requirement is not arbitrary. Reg. Guide 1.60 [7], issued in 1973, gives guidance on the design values of ground

acceleration up to a frequency of 33 Hz. Frequencies above 33 Hz are assumed to be outside postulated seismic events.

Motivation for the study

There remains a practical upper limit to dynamic testing that is imposed by the availability of test equipment. This upper limit is governed by the size of the hydraulic pumps and servo actuators supplying fluid to the actuating test cylinder. At current writing, this limit is approximately an input load of 200 kips @ 33 Hz. New reactor designs, including the Westinghouse AP1000 plants under construction at Vogtle and VC Summer sites, have applications for snubbers with rated loads up to 1900 kips. Functional testing can be conducted on these large units to verify the lockup and bleed parameters are correct, as well as the load carrying capacity. However, the dynamic spring rate of the snubber will not be experimentally verified at full rated load.

The purpose of this study is to develop an FEA model of a hydraulic snubber that can be compared to existing data of tests performed by Anvil Engineered Pipe Supports (EPS). If an accurate model can be developed for smaller snubber sizes, it could be used to determine the spring rate of units that exceed the capacity of existing test equipment.

CHAPTER 3

Dynamic Qualification Testing Conducted By Anvil EPS on Fig. 3306 Hydraulic Snubbers

Anvil EPS developed a second generation snubber in the late 1990's. This snubber is known as a Figure 3306 (Figure 8). At Anvil EPS, each part is given an arbitrary numerical designation, or Figure number. This snubber line has 7 sizes of various strokes, with load ratings from 350 lbf to 120,000 lbf. This study focuses on the size 35 and size 100 models.

Figure 8 – Size 35 Fig. 3306

Common Features:

The Anvil Fig. 3306 sizes 35 and 100 share some common features. They are both cylindrical in shape and have internal fluid reservoirs. The control valves are mounted inside the piston. The size 35 and 100 are different from the rest of the line in that they utilize dual piston rods.

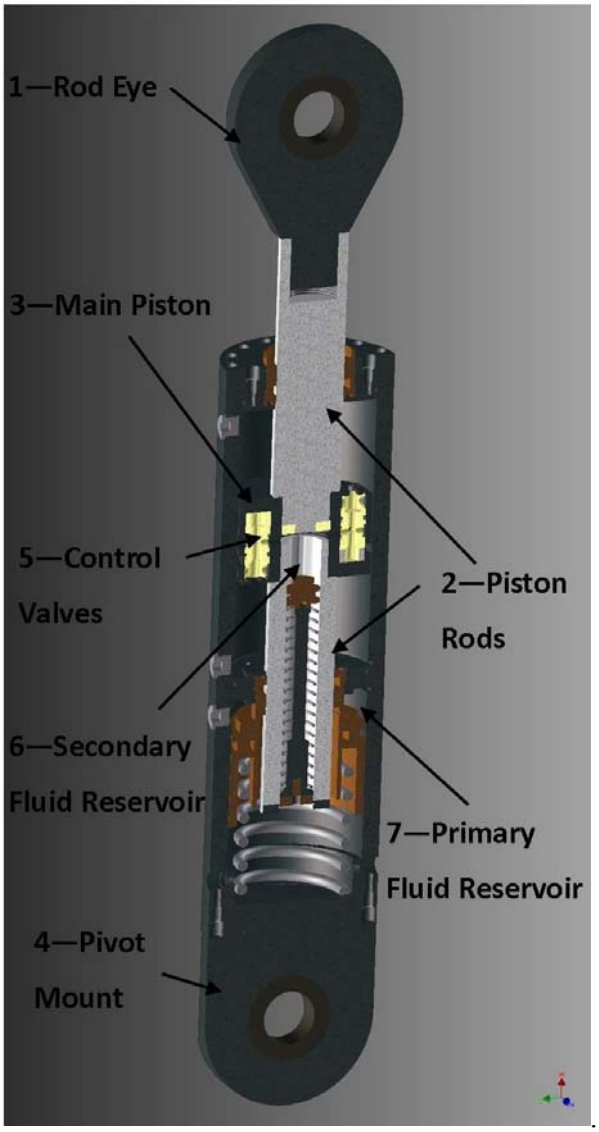

Figure 9 – Fig. 3306 Size 35/100 Cut-Away Rendering

The following description assumes a movement that causes the cylinder piston rod to retract. The rod eye is connected by a pin to the piping or equipment to be

restrained. Movement is transmitted to the piston from the rod eye via the front piston rod. The pivot mount is pinned to a rear bracket, and the piston moves relative to the cylinder. This is known as the compression side. The piston displaces fluid on the compression side, and it flows through the control valves into the tension side. The cylinder and piston dimensions are such that the rod eye can move a magnitude of 6" from the fully retracted position to the fully extended position. This is referred to as cylinder stroke. A piston at mid-stroke can retract or extend 3" relative to the fixed pivot mount.

The rear piston rod is not load bearing but does provide key advantages. It provides more resistance to side loading by keeping the piston aligned in the cylinder under large lateral accelerations. It also equalizes the surface area of the piston on the tension and compression sides, which does two things:

- The primary fluid reservoir can now be sized for thermal expansion/contraction only and does not need to include volume for fluid displacement due to piston rod retraction.
- Deflection of an incompressible fluid column has the same load/displacement relationship as an axially loaded elastic member, or $= \frac{PL}{A\beta}$, where β is the fluid bulk modulus, and P, L, and A are the applied load, fluid column length, and piston area. For single rod hydraulic cylinders, the equation for peak to peak deflection due to the fluid columns under sinusoidal loading is

$$\delta_{fluid} = \frac{P_T L_T}{A_T \beta} + \frac{P_C L_C}{A_C \beta}$$

with the subscripts T and C denoting the tension and compression sides. The lengths of the tension and compression fluid columns add up to the total length

of snubber stroke, or $L_T + L_C = L$. When tension and compression piston areas are equal, fluid deflection simplifies to

$$\delta_{fluid} = \frac{(P_T + P_C)L}{A\beta}$$

and is now no longer a function of piston position.

Materials of Construction

Many different materials go into the construction of a Fig. 3306. The piston, piston rods, and endcap are of carbon steel construction, either SA-36 or A-108 Grades 1018CW thru 1050CW. The cylinder tube is either SA-513 or SA-519, Grades 1018CW thru 1026CW . The cylinder head is made of SA-564 Type 630 age hardened at 1075° F stainless steel. The piston rod and pivot mount are SA-193 Gr. B7 chrome alloy, and the cap screws are high-strength SA-434 Class BC carbon steel.

The pressure differential developed over the poppet valve is partly a function of viscosity, thus snubber activation is also viscosity dependent. The viscosity of the working fluid must be relatively stable through a variety of environmental conditions. The fluid is a silicone polymer known as polydimethyldiphenylsiloxane, and is widely used in many brands of hydraulic snubbers. This silicone based fluid was originally manufactured by General Electric under the brand name GE SF-1154. A critical characteristic of this fluid is its excellent viscosity stability when exposed to radiation. It has been tested by Anvil EPS up to 1×10^9 rads of gamma exposure with no significant gelation. Its viscosity is also fairly stable at elevated temperatures. This provides more consistent functional test results, as field testing is not always done in a temperature controlled setting.

For the load/displacement relationship of interest in this study, fluid bulk modulus is of great importance. As mentioned previously, fluid bulk modulus can vary from batch to batch. At the time Anvil's testing was carried out, Anvil was in the process of qualifying a new fluid vendor, and the lot of fluid used in the qualification tests underwent laboratory analysis to determine the bulk modulus. This laboratory testing was done at 70° F and will be used for this study. For simulations at 200° F, experimental bulk modulus data is not available and historical Anvil data will be used.

Fig. 3306 Qualification Testing to ASME QME/QDR Requirements

The Fig. 3306 is a second generation snubber that was intended to be utilized by new build plants invoking ASME B&PV Design code Section III 2007 or later. A full campaign of qualification testing was conducted at four different labs for all seven sizes, culminating in the 2009 testing of the size 35 and 100. Testing for these sizes was conducted at National Technical Systems in Santa Clarita, CA. Over the course of several months, the full suite of QDR qualification tests were conducted as outlined in Anvil procedure PE 9851-3 [21]. Of particular interest in this study is the test setup in Figures 10 through 13.

Each snubber was pinned at the pivot mount to a fixed bracket and to an actuating hydraulic cylinder at the rod eye. A linear transducer was mounted on the rod eye and cylinder head to measure deflection of the rod eye relative to the cylinder (Figure 11). This configuration does not measure cylinder deflection, and an assumption was made that cylinder axial deflection was minor compared to fluid column deflection. It is worth noting that in this test configuration, in addition to

cylinder deflection in tension, the clearance between the pins, spherical bearings, rear bracket holes, and the pivot mount deflections, are not taken into account.

A load cell was placed in the load path between the actuating cylinder and snubber rod eye. In addition to measuring the load applied to the snubber, the load cell provides feedback for actuator load control. Load control is utilized to prevent the snubber from generating high working pressures inside the cylinder. As the loaded fluid column deflects, the unloaded column will draw fluid from the secondary reservoir to prevent cavitation in the unloaded side. Under displacement control, the additional fluid volume creates a higher pressure and over the course of many cycles, internal pressure can become high enough to cause seal failure. By using load control, this can be avoided.

The rated load of each cylinder is applied by the actuating cylinder with a sinusoidal waveform at frequencies between 1 Hz – 33 Hz. Cylinder load and displacement were sampled at a time increment of .0002 seconds. During testing, it was determined that there was electronic “noise” in the system, and 150 Hz filter was placed on both the load and deflection outputs to filter out high-frequency signals. Data was recorded into LabView software, and made available in a format readable to Microsoft Excel.

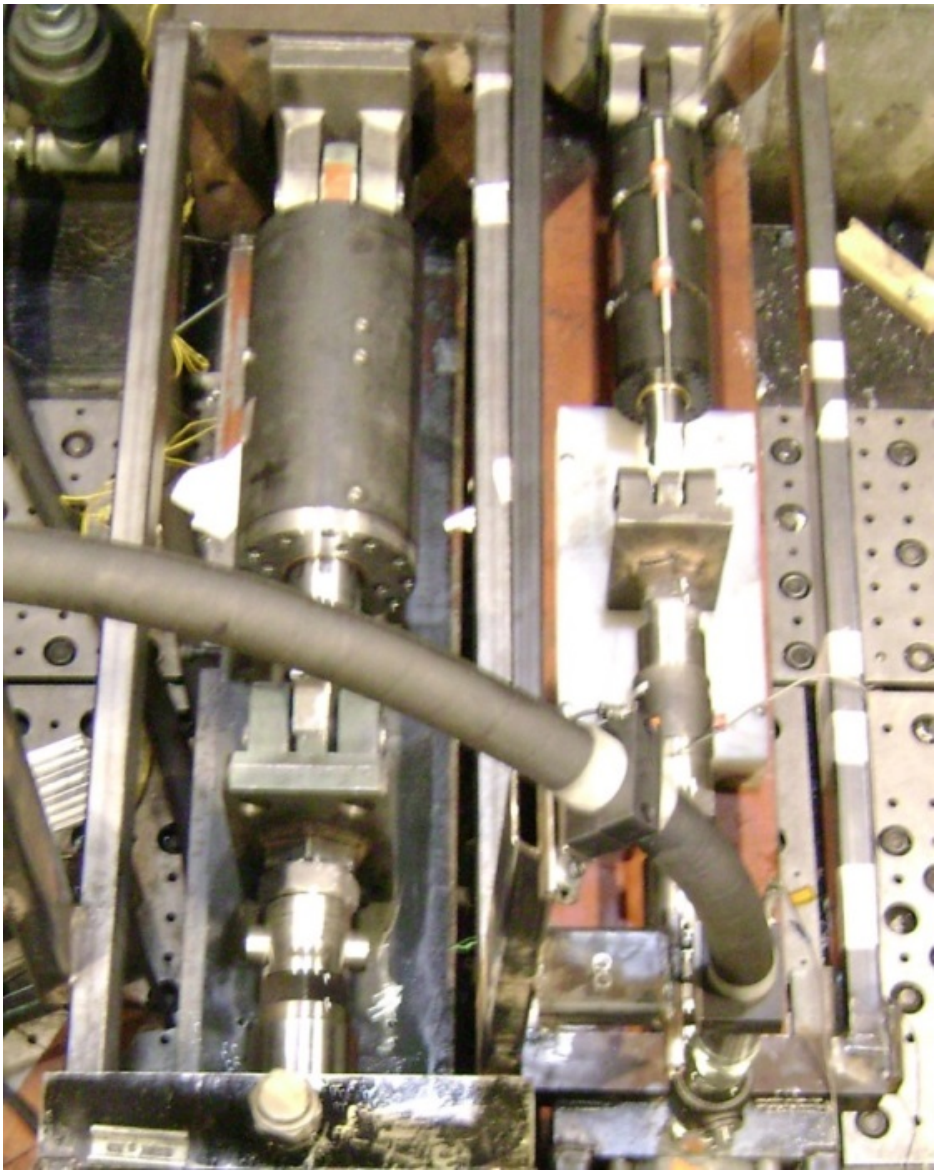

Figure 10 – Size 35 and 100 Fig. 3306 in dynamic test fixtures at National Technical Systems Labs. Richards, Rick, 2009

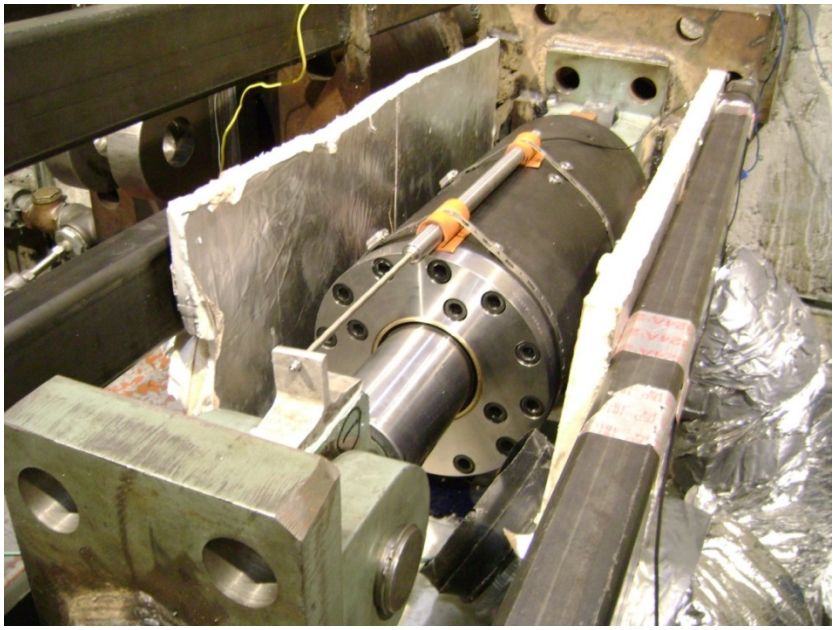

Figure 11 – Size 100 prior to high temperature drag/functional testing. Note the linear transducer banded to the cylinder and mounted to the rod eye. Heat was pumped into a foam board enclosure around the snubber that was used as an insulating layer to maintain a snubber temperature of 200° F. Richards, Rick, 2009

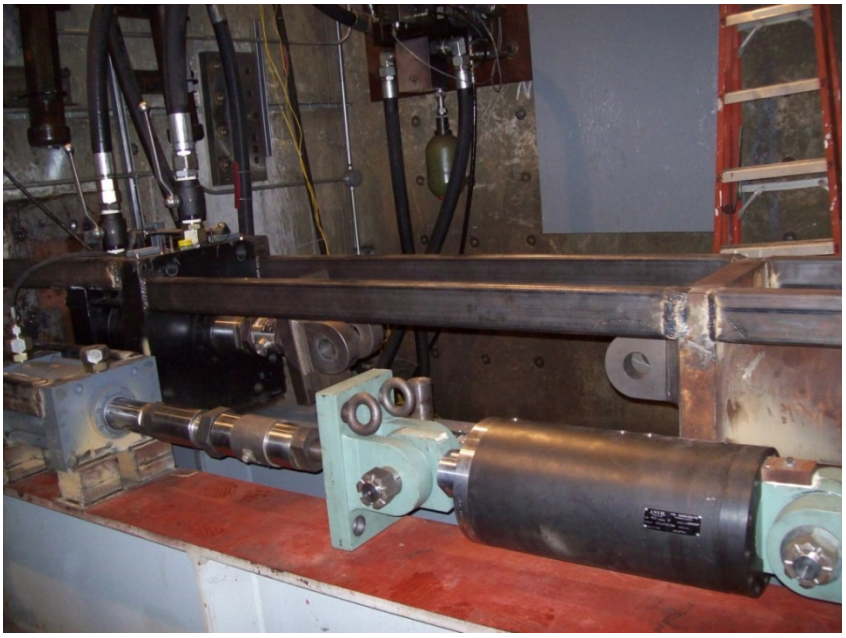

Figure 12 – Size 100 Fig. 3306 in the test setup. NTS Labs had two machines configured for snubber testing, a smaller unit for drag force and functional testing (foreground, with snubber mounted), and a larger machine for high frequency dynamic testing (background). The actuating cylinder and load cells are visible for both test setups on the left hand side of the photo. Richards, Rick, 2009

Figure 13 – Size 35 inside the makeshift "oven" during a high temperature functional test. The size 100 can be seen mounted on the large test machine at the top of the photo. Richards, Rick, 2009

Loading and Deflection Direction Conventions

During the tests, a direction convention was established that cylinder extension is positive, and cylinder retraction is negative. A load applied that causes the cylinder piston to move outward relative to the body is positive and any load that causes piston movement inward relative to the cylinder body is negative. Also, extension and retraction are sometimes referred to as the tension and compression sides. Forces that place the snubber in tension are positive, and forces that place the snubber in compression are negative.

Because the size 35 and 100 cylinders feature a double piston rod, all dynamic testing conducted by Anvil on these sizes took place with the cylinder approximately at mid-stroke, or 3" from full cylinder retraction. The linear transducer to measure

displacements was zeroed at mid-stroke. All displacement values are given relative to this zeroed value. A positive value indicates the piston has extended from mid-stroke; a negative value indicates the piston has retracted.

Test Sequence and Data Reduction by Anvil EPS (PE 9851-6)

The full test sequence conducted by Anvil EPS includes all functional and dynamic testing mandated by QME/QDR. After testing was conducted, the data was reduced by Anvil EPS to come up with numerical values for snubber spring rate. To reduce the data, the following method was employed:

1) Review the raw lab data files using the proprietary NTS Plot File Viewer. This program enables the user to view tab delimited text files and plot values on an X and Y axis. Displacement was plotted on the X axis, and Time on the Y Axis (Fig. 14)
2) Using NTS Plot Viewer, scale the X and Y axis until the extrema of individual cycles are visible in the plot (Fig. 15). Record the start and end times of the cycles that are of interest
3) Open the tab-delimited .dat files in Microsoft Excel.
4) Locate the rows with the cycles of interest in the spreadsheet. Plot load on the primary axis, displacement on the secondary axis for approximately 5-10 cycles.
5) Draw a line of best fit between the maximums of each cycle. Repeat for the minimums of each cycle.

6) Record the values of maximum and minimum displacement where the lines of best fit intersect the secondary axis (Fig 16).
7) Determine spring rate of the cylinder according to QDR-4110(g), or

$$\frac{F_{max}-F_{min}}{\delta_{max}-\delta_{min}} = k$$

As stated previously, the position of the linear transducer does not record lost motion or cylinder/pivot mount deflection. To accurately determine spring rate, these values of deadband and cylinder deflection were calculated and added to the total deflection. The spring rate values published by Anvil EPS reflect this additional deflection. To simplify data reduction, the spring rate values reported in this paper do not reflect lost motion or cylinder/pivot mount deflections. This includes all experimental data presented in this section and simulation outputs presented later.

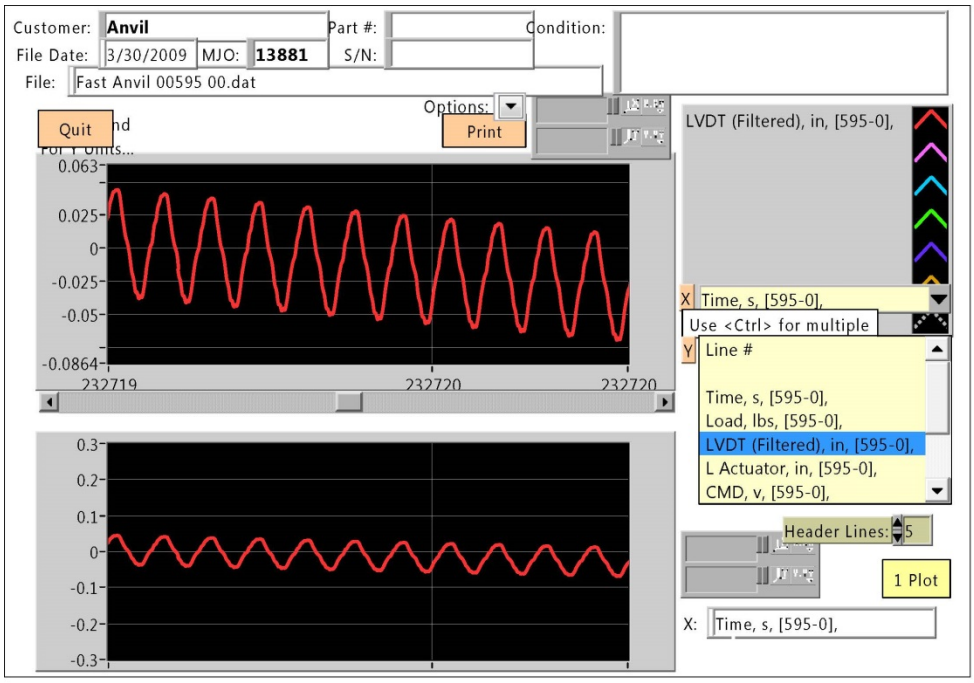

Figure 14 – Zoomed in view of 10 Hz test

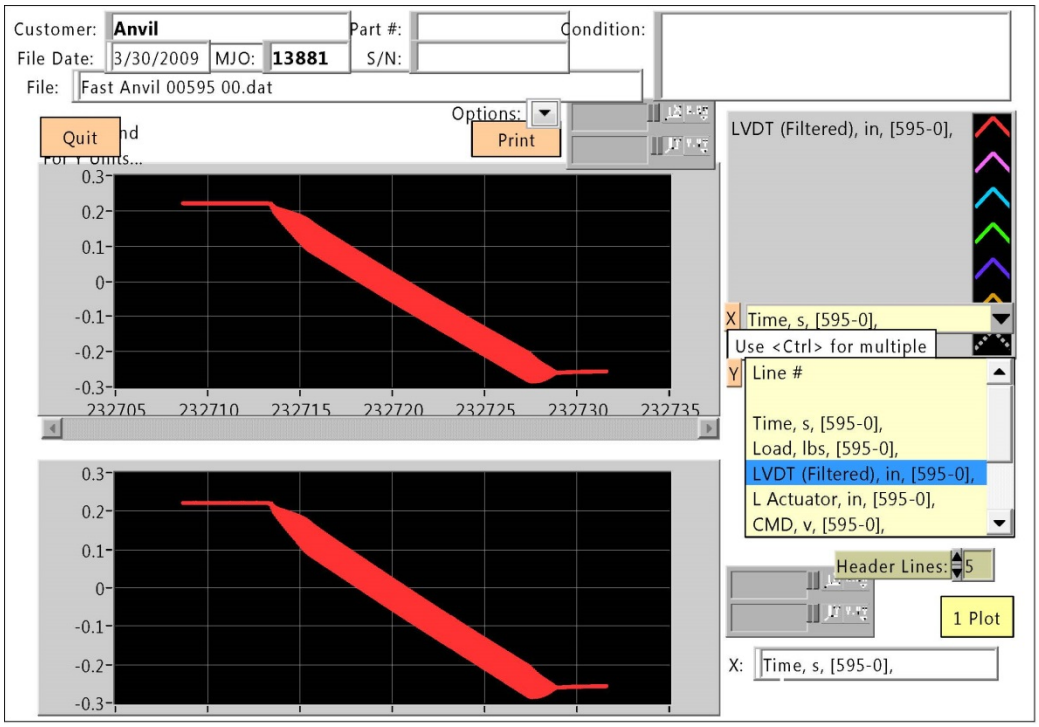

Figure 15 – NTS Plot of an entire test @ 10 Hz

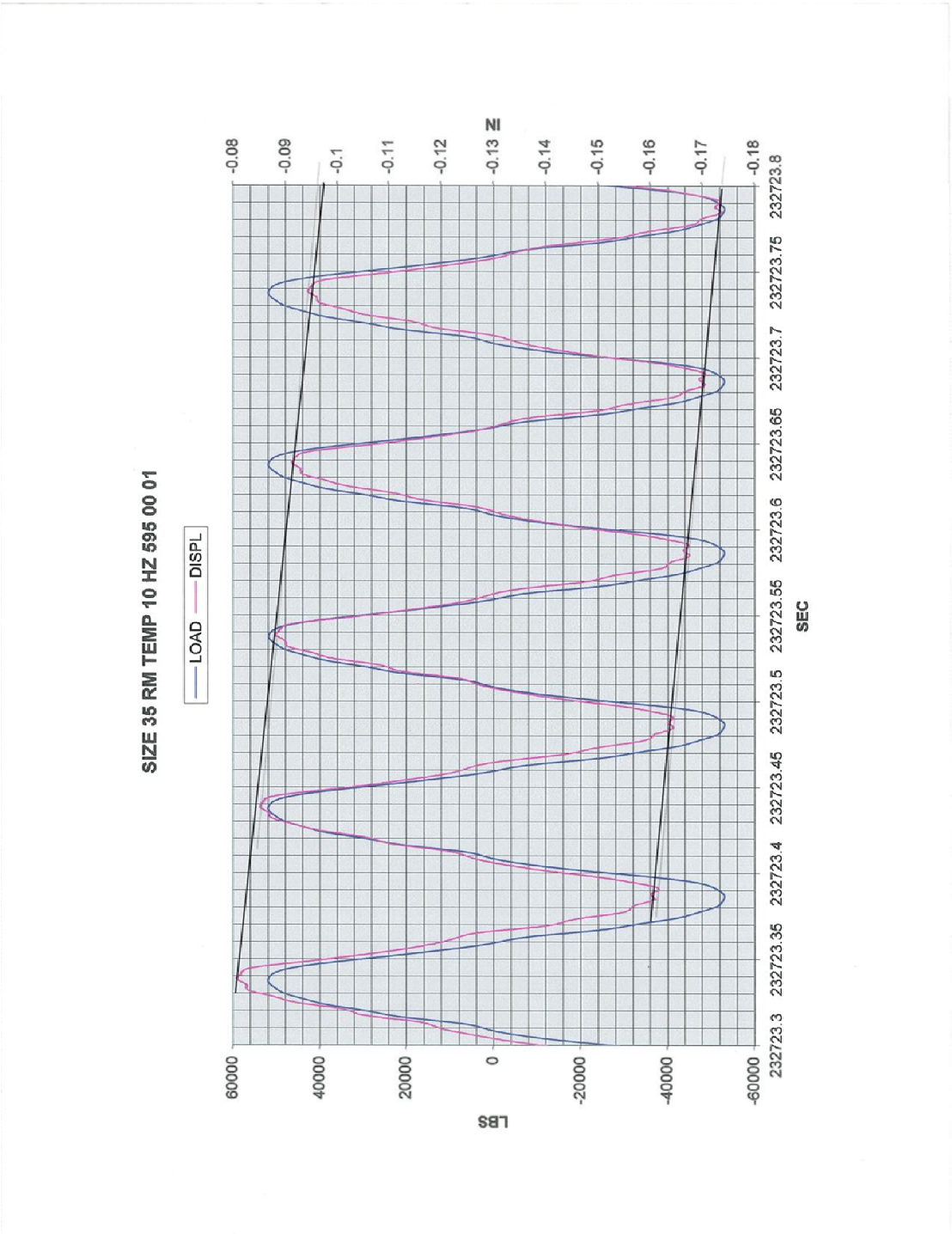

Figure 16 – Same 10 Hz w/ load and deflection plotted against time. Note line of best fit drawn between maximum and minimum and minimum deflections. [15]

Spring Rate Values as Reported by Anvil EPS [15, 16]

Table 1 - Spring Rate Values as Reported by Anvil EPS				
	Spring Rate kips/in			
Freq (Hz)	Size 35 Ambient	Size 35 200° F	Size 100 Ambient	Size 100 200° F
1	1,033	822	1,870	1,827
2	1,248	935	2,102	2,115
3	1,342	997	2,170	2,178
5	1,379	996	2,115	2,026
10	1,346	1,021	2,036	1,915
15	1,259	1,002	1,900	1,760
20	1,195	957	1,761	1,666
25	1,078	1,041	1,758	1,560
30	1,035	811	1,410	1,578
33	940	833	1,431	1,569

Data Reduction Through Use of Computer Code

One of the challenges Anvil faced in reducing the data was the sheer volume of information. As an example, Figure 16 shows 5 cycles of a test that lasted for 12 seconds at 10 Hz, for a total of 120 cycles. The spring rate value was determined by using only 4% of the available data. To some degree, the reduction of the test data is subject to a small bias by selection of different cycles, or to interpretation of the analyst, or where the line of best fit is drawn on a particular day.

To work with a larger set of data and remove graphical interpretation from the equation, code was written in Microsoft Excel Visual Basic for Applications, or VBA to return the extrema for each cycle in the selected time period. The user must still choose a start and end time of the cycles in question; the recorder was on before a load was applied to the system, and the actuating cylinder takes several cycles to ramp up

to the desired load. This can be seen in Figure 15, where it takes approximately 12 seconds to achieve the minimum test load of 100 kips peak to peak, and the last 5 seconds have no meaningful data. Once the start and end times are specified, the start and end of each cycle is periodic as a function of the test frequency. By iterating through each cycle, the maximums and minimums can be extracted for the entire test.

One behavior that is evident in the dynamic test plots is drift of the piston position over the course of the test. In Fig. 15, the initial piston position is approximately .22" extended from mid-stroke. At the end of the test, piston position has experienced some "drift", and traveled to -.25" retracted from mid-stroke. This phenomenon is characteristic of all hydraulic snubbers. The mechanism of drift is not well understood, and is a combination of fluid flow through the check valves and bleed valves under cyclic loading. If the test is long enough, under load control the snubber will reach equilibrium when the stiffness in tension equals the stiffness in compression and the drift will stop.

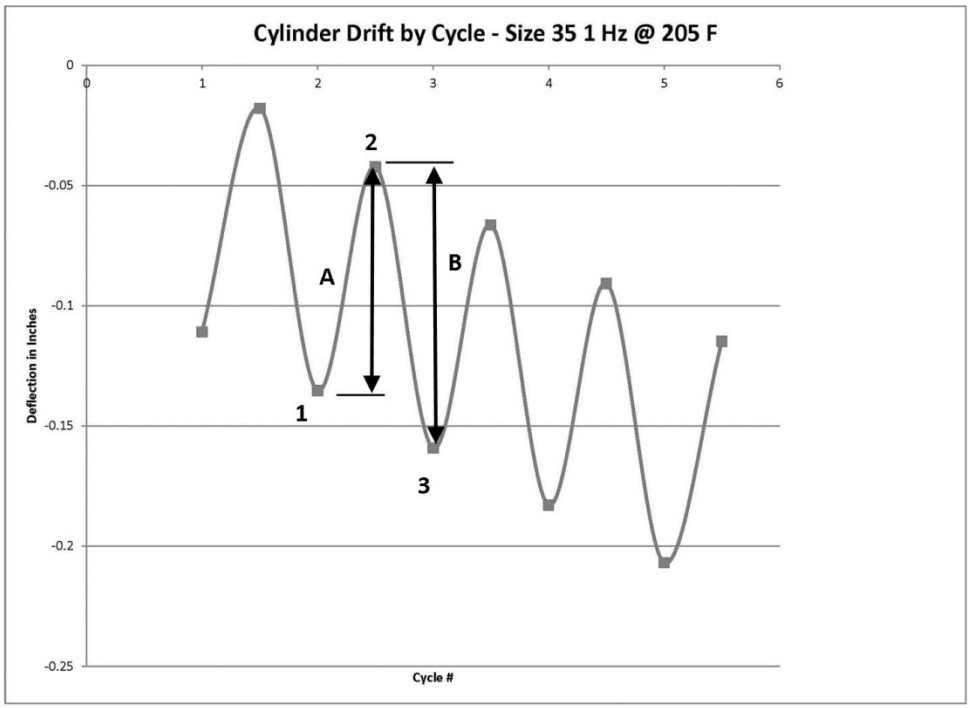

Figure 17 – Cylinder drift @ 1 Hz for the Size 35

An understanding of the drift mechanism is not required for determining spring rate. Fig. 17 plots the displacement extrema of 5 cycles at 1 Hz. Upon inspection, it is apparent that the maximums and minimums of each cycle drift by approximately -.025" each cycle. This "drift" will skew the peak to peak displacements depending on how they are measured. Using the 2nd cycle as an example, measuring the distance A will result in a smaller displacement than measuring peak to peak distance B. Because snubber "drift" happens at a rate that is approximately linear, the peak to peak displacements A and B can be averaged to find the true peak to peak distance.

Summary of Results as Reduced by Computer Code

The spring rates for the Size 35 and 100 at room temperature and 200° F are given in tables 2 through 5 as a function of frequency.

Table 2 - Size 35 Spring Rate @ 70° F			
Frequency (Hz)	Peak to Peak Load (kips)	Peak to Peak Displacement (inches)	Pin-to-Pin Spring Rate (kips/in)
1	104.292	0.1011	1,032
2	103.884	0.0846	1,228
3	102.953	0.0779	1,321
5	102.319	0.0746	1,372
10	105.122	0.0799	1,316
15	103.004	0.0835	1,234
20	102.576	0.0860	1,193
25	102.281	0.0947	1,080
30	106.468	0.1060	1,004
33	103.873	0.1100	944

Table 3 - Size 35 Spring Rate @ 200° F			
Frequency (Hz)	Peak to Peak Load (kips)	Peak to Peak Displacement (inches)	Pin-to-Pin Spring Rate (kips/in)
1	104.501	0.1290	810
2	104.722	0.1146	914
3	103.732	0.1074	966
5	104.965	0.1060	990
10	106.165	0.1065	997
15	104.826	0.1065	984
20	106.917	0.1143	935
25	106.48	0.1072	993
30	104.549	0.1294	808
33	105.278	0.1265	832

Table 4 - Size 100 Spring Rate @ 70° F			
Frequency (Hz)	Peak to Peak Load (kips)	Peak to Peak Displacement (inches)	Pin-to-Pin Spring Rate (kips/in)
1	260.254	0.1452	1,792
2	259.748	0.1257	2,066
3	257.218	0.1187	2,167
5	254.338	0.1280	1,987
10	251.203	0.1318	1,906
15	255.892	0.1441	1,776
20	258.132	0.1568	1,646
25	254.991	0.1632	1,562
30	252.200	0.1587	1,589
33	246.551	0.1557	1,584

Table 5 - Size 100 Spring Rate @ 200° F			
Frequency (Hz)	Peak to Peak Load (kips)	Peak to Peak Displacement (inches)	Pin-to-Pin Spring Rate (kips/in)
1	261.459	0.1390	1,881
2	257.558	0.1228	2,097
3	252.803	0.1181	2,141
5	253.784	0.1222	2,077
10	246.334	0.1239	1,988
15	247.801	0.1306	1,897
20	253.702	0.1471	1,725
25	252.289	0.1466	1,721
30	247.265	0.1720	1,438
33	248.302	0.1714	1,449

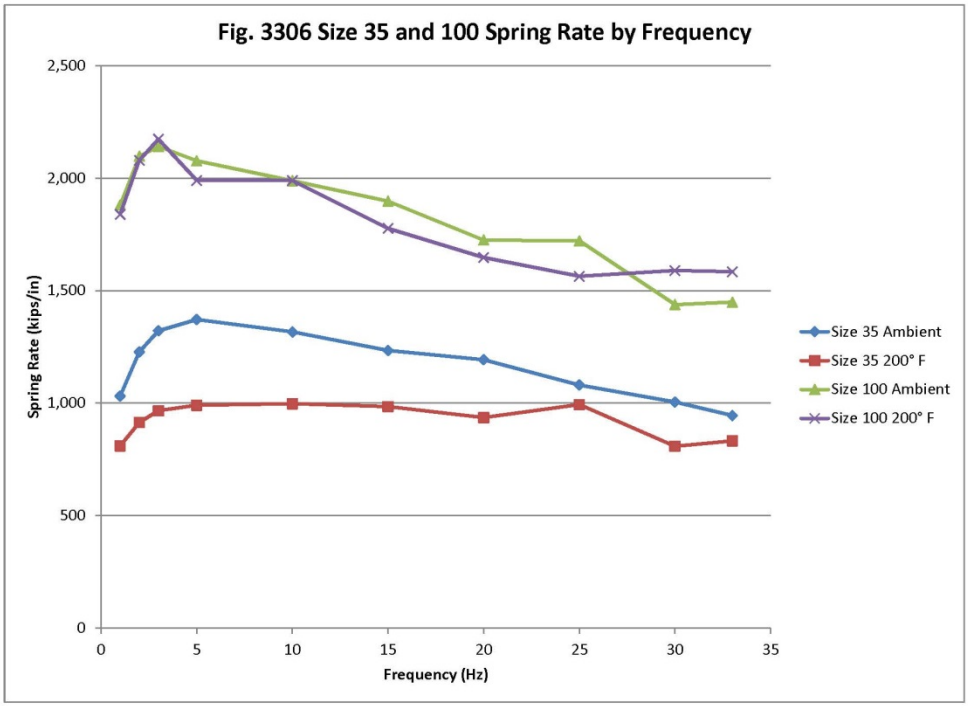

Fig. 18 – Snubber Spring Rate by Frequency, Sizes 35 and 100 from Anvil tests

Interpretation of Test Data

Figure 18 shows two separate sizes, the size 35 and 100, at two different temperatures, 70° F and 200° F, for a total of four test sequences. Each test sequence shows the same behavior; Spring rate reaches a maximum value somewhere between 3 Hz and 10 Hz, with declining values as a function of frequency. The Size 35 and 100 high temperature tests have a lower spring rate than the room temperature tests, as expected. The working fluid, SF-1154, has a bulk modulus that decreases with temperature.

Looking at Fig. 18 in more detail, each test plot shows a sharp increase in spring rate from 1 Hz to 3 Hz. At lower frequencies, these valves spend a larger

percentage of time in the open position, allowing fluid to flow between the tension and compression sides. This fluid flow causes larger displacements, reducing snubber stiffness.

The test data shows a maximum stiffness value at approximately 3 Hz. At frequencies greater than 3 Hz, fluid flow through the check valves is minimal, and it can be assumed there is no fluid flow (aside from drift) between the tension and compression sides. For the size 35, the values of spring rate are relatively constant between 5 Hz – 15 HZ and appear to be independent of frequency in this region. As frequency increases to 33 Hz, the values trend down, indicating a softening of the snubber as frequency increases. For the size 100, this downward trend occurs immediately after a maximum spring rate at 3 Hz.

CHAPTER 4

FEA Simulation of Dynamic Qualification Testing

To develop an analytical model that can be tested against experimental data, an FEA simulation was created using ABAQUS version 6.13, published by the Simulia Corporation. The objective of the simulation is to reproduce the spring rate values in Fig. 18. To this end, both static and dynamic models were developed. The static model is geometrically accurate and used to determine that the units are consistent, the applied load does not grossly deform the cylinder, and the deflections are the expected order of magnitude. The dynamic model is a simple axisymmetric representation of the snubber used to isolate the fluid behavior.

Assumptions

1) No fluid exchange occurs between the tension and compression sides of the cylinder

   It is assumed that the poppet style check valves are in the closed positon the entire length of the simulation, and there is no fluid transfer between the tension and compression sides of the cylinder through the bleed valves. The test data supports that the opening and closing of these valves only has an impact for frequencies lower than 3 Hz, and the frequencies of interest

here are between 3 Hz – 33 Hz. This assumption was made to reduce the number of elements and stay away from the realm of CFD simulations.

2) "Walking" does not occur

A consequence of Assumption 1 is that snubber drift does not occur. The test data shows that this drift adjusts the deflection extrema at a linear rate, and this has been taken into account in the experimental test data reduction. It will not have any impact on the cycle to cycle values of deflection in the simulation.

3) Fluid bulk modulus is not variable w/ pressure

During dynamic cycling, the internal pressure of a snubber will increase above the value due to the applied load. For example, if the snubber cycles first in tension, the compression fluid column will deflect, causing fluid to flow into the tension side from the reservoir. As the snubber moves to a neutral position, the pressure on the compression and tension sides balances at a non-zero value. With no bleed valves, this value asymptotically approaches the pressure that would be present at full load with each cycle. When the snubber is now in a neutral position of zero deflection, it is pressurized in the tension and compression sides at 1 X full load. When a load is applied, the loaded side is at a pressure that is 2 X full load, and the unloaded side is at zero.

In actuality, some of this pressure is bled off through the bleed valves at a pressure dependent rate. There is no test data that shows what actual pressure inside the cylinder is during a dynamic event, and it is assumed that

ΔP between the tension and compression sides is 2 X full load. In the simulation, with Assumption 1, ΔP will still be 2 X full load, although the loaded side will be pressurized to 1 X rated load and the unloaded side will in a vacuum at – 1 X rated load.

4) Fluid deflection governs the response to load

   In the dynamic model, it is assumed that steel deflections are orders of magnitude smaller than the deflection of the fluid. This assumption is valid, as Young's modulus for steel is approximately 150 X the bulk modulus of the hydraulic fluid.

Fluid Cavity Material Models

Two material behaviors were developed for the fluid cavity:

1) Fluid Cavity Interaction

   This behavior models a fluid cavity as a linear elastic volumetric spring [18], with properties of density and bulk modulus. A fluid cavity is defined by an enclosed surface with normal pointing inward. The elements are surface elements, but they are coupled to a cavity reference node that has properties of pressure and volume. As the surface elements deform due to an external load or internal pressure, the pressure and volume properties of the reference node are updated to the new conditions. These properties are then applied to the next step or increment. This interaction can be used with both implicit and explicit static and dynamic procedures.

2) Hydrodynamic Equation of State

This material model can be used to simulate both compressible and viscous behavior. ABAQUS provides several examples utilizing a linear Mie-Grüneisen equation of state to model discretized fluid deformation [18]. Energy is dissipated either through volumetric or shear deformation. The user must specify density, viscosity, and the speed of sound through the material, which is a function of bulk modulus and density.

Output from the fluid cavity interaction and the equation of state model agree within a few percentage points. The data presented in the output section uses the cavity interaction for the static model, and equation of state for the dynamic model. Discretizing the fluid as acoustic elements was also examined with very similar results to the other two material models.

Choice of Procedures

The general/static procedure was chosen for the static model primarily for ease of use in creating a complicated model of linear elastic behavior. Several iterations of the model were developed, beginning with a very simple fluid cavity and cylinder with an applied load that did not vary with time. The outputs of the simulation could then be verified by hand. As more complicated elements were added to the model, the model behaviors could be quickly compared to the test data or an expected result.

For the dynamic model, the explicit/dynamic procedure is used. This procedure satisfies equations of motion at increment n, and uses the acceleration of that increment to advance the model to the next n + 1 increment. The explicit dynamics

procedure allows for a time history of linear response to be modeled. It has been verified through testing that the natural frequency of the size 35 and size 100 snubbers does not exist in the frequencies of interest, therefore all load/deflection response is expected be linear.

A consequence of using this procedure is the required time increment can be very small compared to the static simulation and can lead to long run times for the same model. The minimum time increment is the time required for the dilatation wave to pass through the smallest element in the model [18]. Complicated geometries that cause large elements to distort or require small elements for an accurate model can decrease the time increment by orders of magnitude for the rest of the model, greatly increasing run times. This drove some differences in the static and dynamic models to keep run times on the order minutes. It is worth noting that implicit dynamic and modal based procedures were also tried, with similar results.

Static Model Geometry

The first simplifying assumption in the model is recognizing that the hydraulic cylinder is round, and the number elements can be reduced by using symmetry. The pivot mount and rod eye are both rectangular in shape, and because of this ¼ symmetry was used in the XY and YZ planes. The cylinder is oriented so the Y axis is parallel with the axis of the snubber cylinder. +Y is cylinder extension, and –Y is cylinder retraction. The Fig. 3306 consists of hundreds of individual parts. In order to reduce the number of contact interactions and elements, many subassemblies were merged together to form continuous pieces. This model consists of 6 parts:

1) Cylinder – Modeled as a 3D solid. For the Size 35, the cylinder ID is 5" and the wall thickness is .5", and with a thickness to ID ratio of .1, a thin-walled cylinder model could be used. However, the Size 100 has a ratio of .125, and the assumption of a thin walled cylinder cannot be made. In order to achieve consistency between the 35 and 100 simulations, they were modeled as solids. Partitions to the internal diameter surface had to be made to accurately describe the fluid cavities. There are also bolt holes at the cylinder ends (Fig. 19).
2) Cylinder Head – Modeled as 3D solid. This part is part of the cavity surface boundary and includes bolt holes (Fig. 20)
3) Cylinder End Cap – Modeled as a 3D solid. This piece is only modeled so as to include bolts and the threaded connection of the pivot mount to the cylinder. Included in the model are the bolt holes (Fig. 21)
4) Pivot Mount – Modeled as 3D solid. This piece is used for the boundary conditions at the pin hole (Fig. 22).
5) Piston and rod assembly – Modeled as a 3D solid. A partition was made in the rod eye to apply a load, and in the piston rods to describe the fluid cavity (Fig. 23)
6) Bolts – Modeled as 2D wire features. These bolts were modeled as wires to reduce the number of elements in the model. They are partitioned to include a node for a bolt pre-load force.

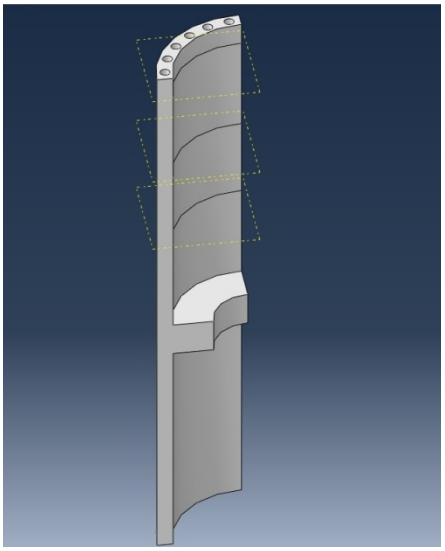

Figure 19 - Cylinder

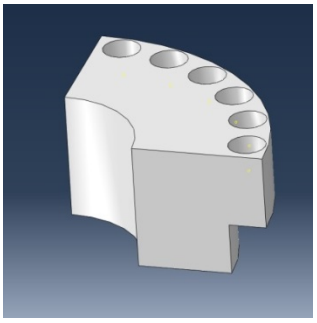

Figure 20 - Cylinder Head

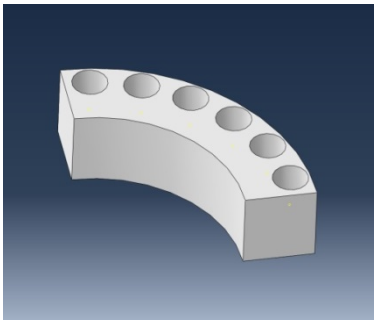

Figure 21 – Cylinder Endcap

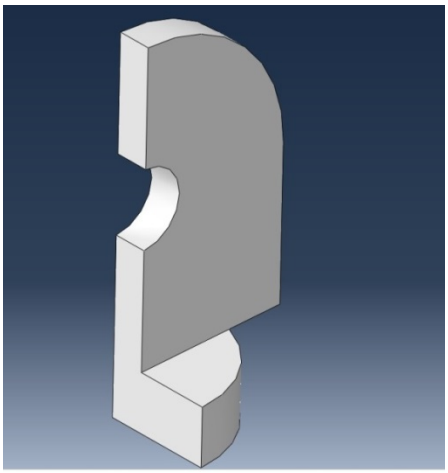

Figure 22 Pivot Mount

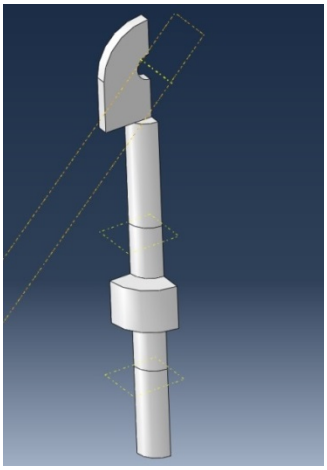

Figure 23 – Piston and Piston Rod Assembly

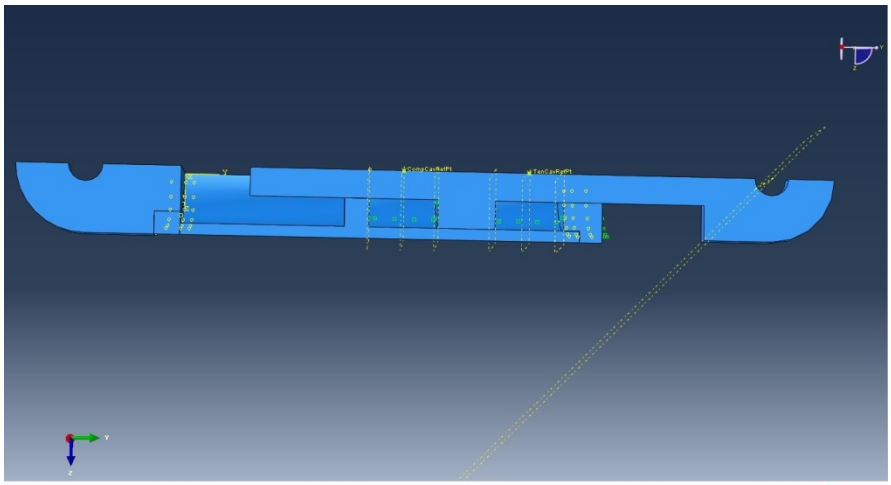

Figure 24 – Size 35 Assembly

Materials – Static Model

The steel parts were modeled as homogenous, isotropic materials. 4 different grades of steel were used in the model. Density and Poisson's ratio are the same for all four, with Young's modulus having slightly different values. The material properties are as follows [17]:

Poisson's Ratio: .3

Density: $7.35 \times 10^{-4}\ \frac{lbf \cdot s^2}{in^4}$

E Low Carbon Steel (< .3%): $29.2 \times 10^6\ \frac{lbf}{in^2}$

E High Carbon Steel (> .3%): $29.4 \times 10^6\ \frac{lbf}{in^2}$

E Low Chrome Alloy: $29.6 \times 10^6\ \frac{lbf}{in^2}$

E 17-4 Stainless Steel: $28.5 \times 10^6\ \frac{lbf}{in^2}$

A variation in Young's modulus and density with temperature will have minimal effect on the model, and was not considered.

The silicone hydraulic fluid has properties of density and bulk modulus in the model. Assumption 3 states that for the purposes of the model, the bulk modulus is not pressure dependent. The values used in each simulation are determined by the pressure at rated load. These values are

Bulk Modulus @ 70° F = $1.98 \times 10^5 \ \frac{lbf}{in^2}$

Bulk Modulus @ 200° F = $1.46 \times 10^5 \ \frac{lbf}{in^2}$

Density @ 70° F = $9.822 \times 10^{-5} \frac{lbf \cdot s^2}{in^4}$

Density @ 200° F = $8.949 \times 10^{-5} \frac{lbf \cdot s^2}{in^4}$

The units of density are not in $\frac{lbm}{in^3}$ as is more commonly seen in literature and reference books. This is a consequence of the choice of units of the applied load and geometry. Inches were chosen as the fundamental unit of length for ease of solid modeling, and units of lbf were chosen as units of force. From $F = ma$, units of mass are now $\frac{lbf \cdot s^2}{in}$ and density is $\frac{lbf \cdot s^2}{in^4}$. To convert $\frac{lbm}{in^3}$ to the correct units, divide by the conversion factor

$$g_c = 32.17 \frac{lbm - ft}{lbf - s^2} \cdot \frac{12\ in}{ft}$$

Static Model Interactions and Constraints

For the static model, the master/slave surface contact definition was used for all interactions of solid parts that come into contact. In this contact definition, pressure is transmitted between the two surfaces. The slave surface is not allowed to penetrate the master surface, although both surfaces are allowed to deform. Friction is not

expected to have a significant effect in the model, so frictionless behavior was used. The fluid cavity interaction was used for both the tension and compression cavities. The cavity reference nodes lie on the axis of the cylinder. There is also a tie constraint between the pivot mount and the cylinder end cap. This constraint ties the movement and rotation of the nodes on both surfaces together via the master/slave relationship.

To simulate the bolted connections of the cylinder head and endcap to the cylinder, multi-point beam constraints were used. This constraint ties the displacement and rotation of a single control point to the nodes that lie on a slave surface. They are connected by an idealized rigid beam. The wire bolt features had two multipoint constraints; One from the bolt "head" to the counter-bored surface, and a second from the threaded end to the internal threads of the cylinder.

Static Model Boundary Conditions

There are four boundary conditions applied to the model

1) Symmetry in the XY plane
2) Symmetry in the ZY plane
3) Fixed surface at the pivot mount pin
4) Fixed X and Z translation at the rod eye exterior flat plane. This is to prevent any moment developing around the fixed pivot mount surface. In actuality, these nodes would be part of a pinned connection and no moment would develop.

Static Model Applied Loads

1) Bolt preload

   This load is applied to an internal node of the wire features used for bolts. This load is applied during the first step after the initial step to determine the deformed lengths of the bolts under the pre-load. This deformed length is then applied to step 2.

2) Primary Loading of the Cylinder

   This load is the applied load to the rod eye and simulates a pin applying a distributed load over 45° of the rod eye ID (Fig. 25). Due to ¼ symmetry, the magnitude of the load will be ¼ the experimental test value. Because it is a pressure distribution acting over 45°, the input magnitude will be greater than the actual value according to the equation

$$Input\ Load = \int_0^{\pi/4} \frac{4}{\pi} \cdot Test\ Load \cos(\theta)\, d\theta$$

   This amounts to an increase of 1.111 for the simulation input from the actual test load. The portion of the load not directed down the axis of the snubber will cancel due to symmetry. There is no input waveform for the static model. It is applied instantaneously in compression in one step, and in tension in a second step.

Static Model Mesh

ABAQUS has a mesh generation algorithm that has a parameter known as seed size. The algorithm places nodes on the model edges, and these nodes are the seed nodes. Seed size refers to the spacing between these nodes, and when possible, node spacing maintains this value throughout the model. ABAQUS suggests a default seed

size based on part geometry and element type. Contact models work best with elements of similar size, so the smallest default seed size was used for the entire model. This is governed by the cylinder head and endcap, which have a default seed size of .42 for the size 35 model, and .71 for the size 100. General purpose continuum elements were utilized. Due to the complex geometries, quadratic tetrahedral C3D10 elements were selected. Various seed sizes were tried, both larger and smaller, and the default provided results that were good enough at a reasonable computational cost. (Fig. 26). For the bolts, B31beam elements with a seed size of .062 and .069 were used.

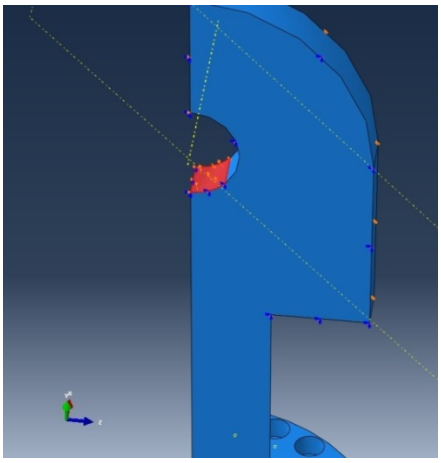

Figure 25 – Applied Pressure Load of Static Model

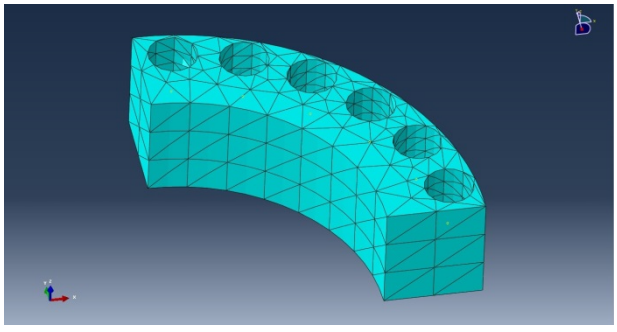

Figure 26 – Cylinder Endcap Mesh

Dynamic Model Geometry

To isolate the fluid behavior, a very simple axisymmetric model was created. Because of Assumption 4, the rod eye and cylinder portion between the compression cavity and the pivot mount could be neglected. This model consisted of three parts, all modeled as planar shells:

1) Cylinder

   Models the cylinder and head as one piece. The interior edge was partitioned to specify cavity surfaces.

2) Piston and Rod Assembly

   Models the piston and piston rods as one piece. To more accurately model the mass of the part, the interior portion of the rear piston rod was removed for the secondary reservoir cavity.

3) Fluid

   Discretized rectangle.

Dynamic Model Materials

For simplicity, only one steel material was modeled. It has the following properties:

Poisson's Ratio: .3

Density: $7.35 \times 10^{-4}\ \frac{lbf \cdot s^2}{in^4}$

E @ 70° F: $29.0 \times 10^{6}\ \frac{lbf}{in^2}$

E @ 200° F: $28.0 \times 10^{6}\ \frac{lbf}{in^2}$

Variations in Young's modulus with temperature were applied in this model, as it will change the speed of wave propagation through the steel parts. Density varies less than 1% with from 70° F to 200° F, and this was neglected.

The fluid is modeled using the equation of state material model. It has the following properties:

Wave Speed @ 70° F: $44773\ \frac{inches}{s}$

Wave Speed @ 200° F: $39706\ \frac{inches}{s}$

Viscosity @ 70° F: $9.827 \times 10^{-5}\ psi \cdot s$

Viscosity @ 200° F: $3.6 \times 10^{-6}\ psi \cdot s$

Density @ 70° F: $9.822 \times 10^{-5}\ \frac{lbf \cdot s^2}{in^4}$

Density @ 200° F: $8.949 \times 10^{-5}\ \frac{lbf \cdot s^2}{in^4}$

Dynamic Model Interactions, Constraints, Boundary Conditions, Loadings

The dynamic model contained no interactions. To enforce continuity between the fluid and steel, a tie constraint between the nodes on the edge of the discretized fluid cavities and the steel cavity surface was created. (Figure 27) The fluid edges were the slave surface. This constraint models the no-slip condition of Newtonian fluids, where the fluid nodes on the interface of the steel-fluid boundary share displacement of the steel.

The only boundary condition needed to prevent rigid body motion is a fixed cylinder base where it would extend to the pivot mount. (Figure 28). The load is applied as a pressure on the main piston rod. It has a sinusoidal amplitude of the form

$$Load(t) = P \cdot \sin(\omega t)$$

This load was applied for .5 seconds for 3 Hz to 5 Hz and .25 seconds for frequencies between 10 Hz and 33 Hz.

Dynamic Model Mesh

The dynamic model is more sensitive to changes in mesh density. The fluid is a much softer material than the steel, and must be a much finer mesh. For the size 35, the piston rod had a seed size of .5, the cylinder .25, and the fluid .15. The size 100 had elements of .75, .5, and .3 respectively. The steel and fluid of both models used axisymmetric solid CAX4R elements.

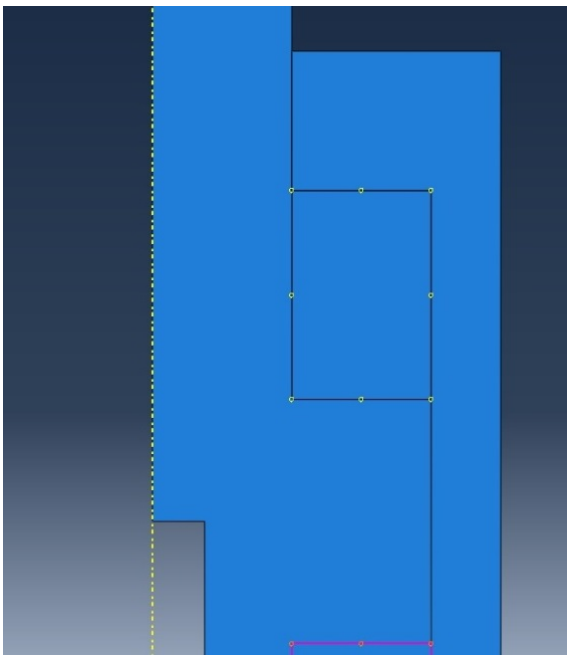

Figure 27 – Cavity Tie Constraint

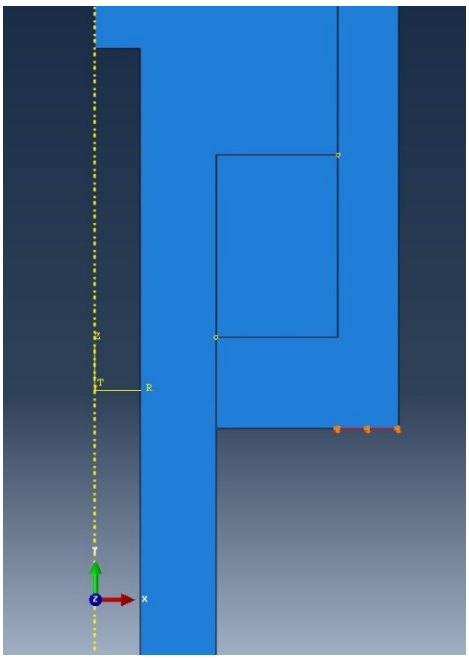

Figure 28 – Fixed Cylinder Edge

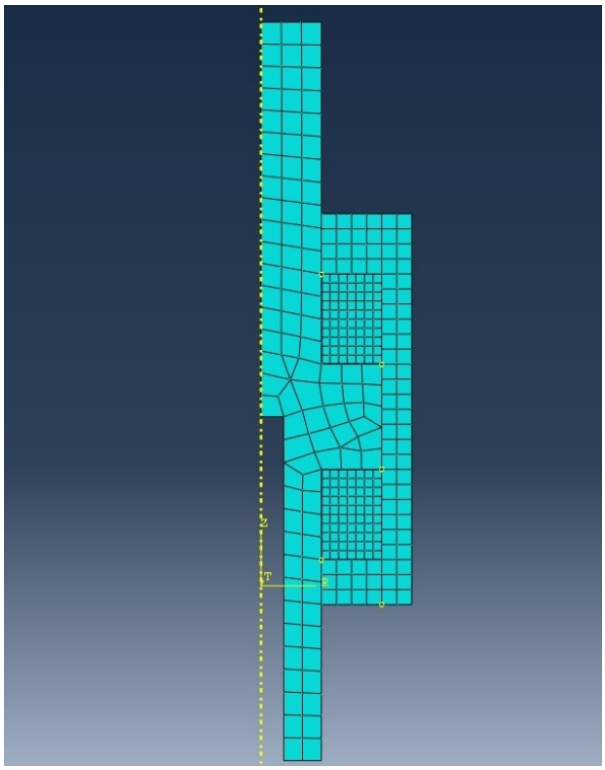

Figure 29 – Dynamic Model Assembly and Mesh

Output

The output of the static and dynamic models includes the deflection of the piston rod and the reaction forces from the fixed axial constraint. These constrained nodes lie on the pivot mount in the static model, and on the cylinder in the dynamic model. In the static model, loading takes place over two steps of time increment 1. In the dynamic model, values were written to the output database at time increments of .0004 seconds for 3 Hz and 5 Hz and .0002 seconds for 10 Hz – 33 Hz. The deflection of the piston rod relative to the fixed cylinder was measured from the motion of a single node on the axis of symmetry.

In the Fig. 3306 qualification testing, there was not much variation cycle to cycle of the input load. This is a consequence of the load controlled nature of the test.

Therefore, to determine spring rate, the maximum magnitude of the input load can be doubled to obtain the peak to peak load. This is divided by the peak to peak deflection. The reaction forces of the nodes fixed in the axial direction relative to the snubber can be summed. The difference in the summed reaction forces and the input load show the inertia effects of the piston/piston rod mass moving with high accelerations.

CHAPTER 5

Static and Dynamic Simulation Results

Static Results

The static spring rates from the ABAQUS models are shown in Table 6

Table 6 - Static Spring Rate As Determined by Simulation

	Temperature	Input Load (kips)	Peak to Peak Deflection (inches)	Static Spring Rate (kips/in)	% Deviation 3 Hz Experimental
Size 35	70° F	52.210	0.0683	1,529	16%
	200° F	52.210	0.0874	1,195	24%
Size 100	70° F	127.465	0.0676	3,771	74%
	200° F	127.465	0.0859	2,968	39%

It was assumed in the experimental data that at 3 Hz, the activation valves were closed and had no effect on piston deflection. The spring rate at 3 Hz is as close to static as the experimental data can get. When measured against the static model, it appears that the values are not in agreement. However, this discrepancy can be explained by the configuration of the reservoir and compression cavity.

The low pressure primary fluid reservoir is sealed off from the high pressure compression fluid cavity with elastomeric seals seated in concentric plates (Figure 30). These concentric plates are held in place by internal retaining rings (Figure 31). On the size 35, these retaining rings are .109 ± .003 inches thick, and the retaining ring groove is .123 ± .002 inches wide. With no tolerances taken into account, with one ring there would be a gap of .014”. The gap caused by two retaining rings plus the tolerance stackups of the concentric seal seats creates uncertainty in the length of the

fluid reservoir. When the cylinder cycles in tension, the compression cavity goes to zero pressure, and the primary reservoir spring pushes the seal seats towards the tension cavity. As soon as the pressure in the compression side climbs above the reservoir pressure, the seal seats move towards the pivot mount, which causes the entire cavity to drift and adds lost motion to the cycle. On the size 100, the gap of one ring is .026”

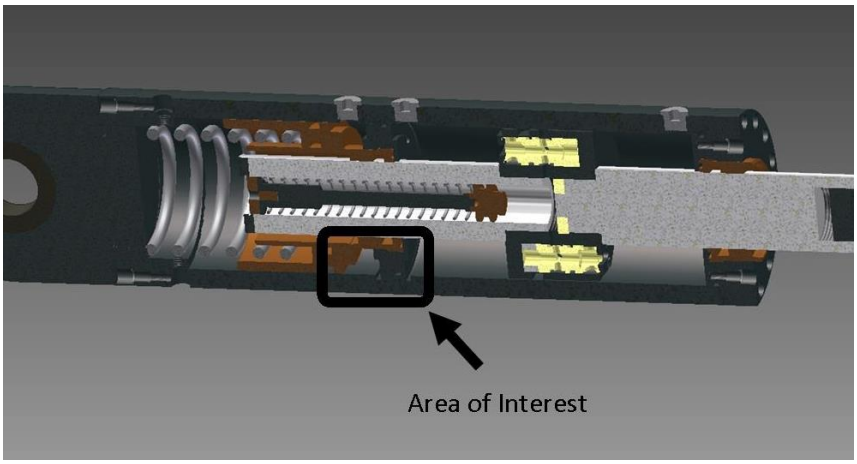

Figure 30 – Location of Concentric Seal Seats

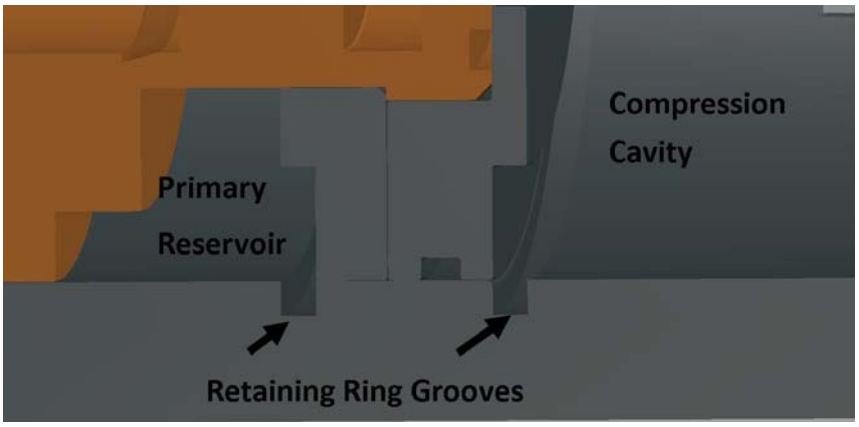

Figure 31 – Retaining Ring Grooves

In the ABAQUS model, the seal gland disks were modeled rigidly connected to the cylinder, and not floating between two retaining rings. When two gaps are added to the peak to peak static deflection, the resulting static spring rate is shown in Table 7

Table 7 - Static Spring Rate with Retaining Ring Gaps

	Temperature	Input Load (kips)	Peak to Peak Deflection (inches)	Static Spring Rate (kips/in)	% Deviation 3 Hz Experimental
Size 35	70° F	52.210	0.0963	1,084	-18%
	200° F	52.210	0.1154	905	-6%
Size 100	70° F	127.465	0.1196	2,132	-2%
	200° F	127.465	0.1379	1,849	-14%

These values are in much closer agreement with the experimental data. The values of % Deviation at 3 Hz are negative because with the retaining ring gaps, the simulated stiffness is less than the experimental data. Without measuring the actual thickness and widths of the retaining rings, retaining ring grooves, and seal seat disk thickness, the amount of lost motion cannot be known. To determine the minimum static spring rate through simulation, the maximum gap width and minimum thicknesses should be summed and included as lost motion. This lends further validity to Assumption 4, that the deformation of the metal parts under load is minor compared to the fluid behavior and now also the manufacturing tolerances and installation clearances in the seal seat assembly and pinned connections.

Dynamic Simulation Results

The dynamic simulation results utilizing the equation of state material model and a dynamic explicit procedure are as follows in Tables 8and 9

Table 8 - Size 35 Dynamic Spring Rate				
Peak to Peak Input Load of 104.065 kips				
	70° F		200° F	
Frequency	Peak to Peak Deflection (inches)	Spring Rate (kips/in)	Peak to Peak Deflection (inches)	Spring Rate (kips/in)
3	0.0776	1,341	0.1003	1,038
5	0.0777	1,339	0.1006	1,034
10	0.0783	1,329	0.1014	1,026
15	0.0788	1,321	0.1022	1,018
20	0.0795	1,309	0.1032	1,008
25	0.0801	1,299	0.1040	1,001
30	0.0805	1,293	0.1049	992
33	0.0809	1,286	0.1053	988

Table 9 - Size 100 Dynamic Spring Rate				
Peak to Peak Input Load of 252.081 kips				
	70° F		200° F	
Frequency	Peak to Peak Deflection (inches)	Spring Rate (kips/in)	Peak to Peak Deflection (inches)	Spring Rate (kips/in)
3	0.0702	3,591	0.0898	2,807
5	0.0702	3,591	0.0903	2,792
10	0.0709	3,555	0.0911	2,767
15	0.0714	3,531	0.0917	2,749
20	0.0719	3,506	0.0922	2,734
25	0.0726	3,472	0.0932	2,705
30	0.0730	3,453	0.0942	2,676
33	0.0731	3,448	0.0949	2,656

Mechanical gaps were not included in the peak to peak deflections. Assumption 4 states that deformation of the steel cylinder is minor compared to the larger fluid deflections, and can be ignored. This means that variations in geometry

between the axisymmetric dynamic model and the experimental test data can be ignored as long as the fluid behavior is modeled accurately. Using 3 Hz as the frequency where spring rate is near static, Table 10 shows that the values for "static" spring rate are the correct order of magnitude and the axisymmetric model is realistic. Arbitrarily adding mechanical gaps or altering geometries of the steel components will not make the dynamic results any more or less valid.

Table 10 - Snubber Dynamic Spring Rate @ 3 Hz

Snubber Size	Temperature (°F)	Simulation Spring Rate (kips/in)	Experimental Spring Rate (kips/in)	% Difference
35	70	1,341	1,321	2%
	200	1,038	966	7%
100	70	3,591	2,167	66%
	200	2,807	2,141	31%

To compare the effect of frequency on spring rate between the experimental data and simulation outputs, dimensionless spring rates can be calculated, with 3 Hz equal to 1. The data is presented in tabular form for the Size 35 and Size 100 in tables 11 and 12, and graphically in Figures 32 and 33

Table 11 - Size 35 Dimensionless Spring Rates				
	Simulated		Experimental	
Frequency	70° F	200° F	70° F	200° F
3	1.0000	1.0000	1.0000	1.0000
5	0.9987	0.9966	1.0383	1.0251
10	0.9911	0.9887	0.9966	1.0319
15	0.9848	0.9810	0.9338	1.0187
20	0.9761	0.9715	0.9029	0.9683
25	0.9688	0.9640	0.8176	1.0282
30	0.9640	0.9557	0.7603	0.8364
33	0.9592	0.9521	0.7148	0.8615

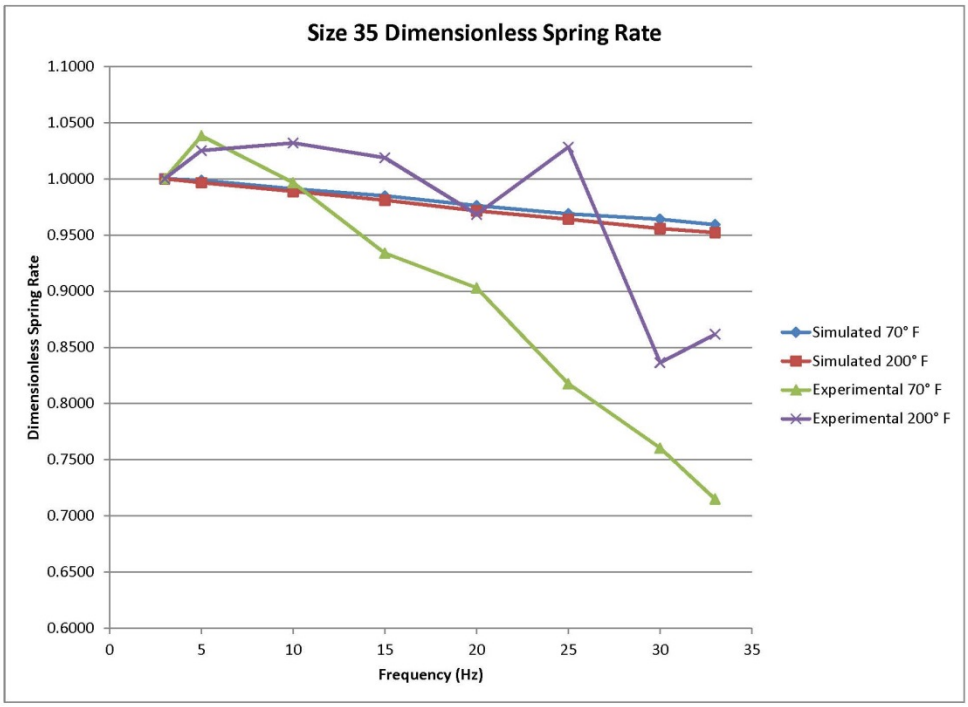

Figure 32 – Size 35 Dimensionless Spring Rate

Table 12 - Size 100 Dimensionless Spring Rates				
	Simulated		Experimental	
Frequency	70° F	200° F	70° F	200° F
3	1.0000	1.0000	1.0000	1.0000
5	1.0000	0.9945	0.9169	0.9700
10	0.9901	0.9858	0.8795	0.9286
15	0.9832	0.9793	0.8195	0.8862
20	0.9763	0.9740	0.7597	0.8056
25	0.9669	0.9636	0.7210	0.8038
30	0.9616	0.9533	0.7333	0.6715
33	0.9603	0.9463	0.7307	0.6766

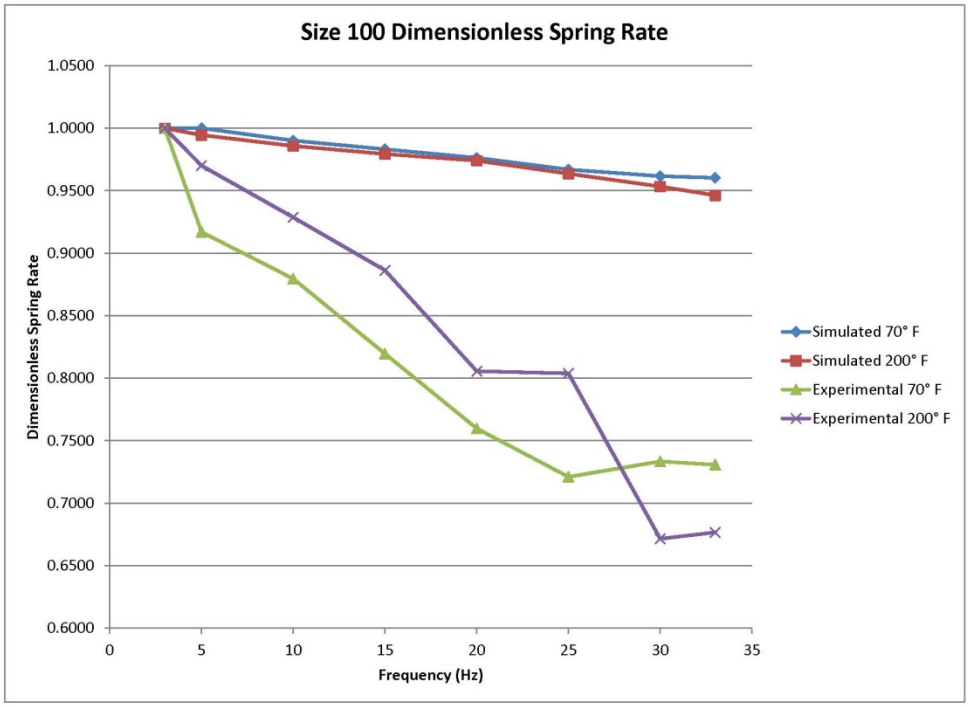

Figure 33 - Size 100 Dimensionless Spring Rate

Discussion of Dynamic Test Results

The frequency dependence of spring rate in the experimental data is much greater than the simulation. Experimentally, the difference in spring rate between 3 Hz and 33 Hz is approximately 30%, and in the simulation is less than 6%. The 6% deviation in the simulation is due to the inertia of the piston and piston rod assembly. This inertia can be seen by measuring the reaction forces of the fixed nodes at the cylinder wall. When the reaction forces in the direction of the applied load are summed, the value is larger than the maximum value of the sinusoidal input.

Inertia should be seen in the experimental data. Under load control, the applied force ramps up at a higher rate for each cycle, causing larger accelerations of the actuator ram and thus larger inertial forces. The simulation data confirms this; Maximum accelerations at 3 Hz for the size 35 room temperature simulation is 250 $\frac{ft}{s^2}$, and 2870 $\frac{ft}{s^2}$ at 33 Hz. However, the experimental data shows no discernable increase in input load as a function of frequency. Table 13 shows dimensionless load as calculated from the reaction forces of the fixed nodes in the simulation, and as measured from the load cell in the experimental data. Figure 34 shows this graphically. There is a linear increase in reaction forces in the simulation, but no pattern in the experimental data.

Table - 13 Dimensionless Load				
	Size 35 @ 70° F		Size 100 @ 70° F	
Frequency	Simulated	Experimental	Simulated	Experimental
3	1.0000	1.0000	1.0000	1.0000
5	1.0018	0.9938	1.0009	0.9888
10	1.0102	1.0211	1.0118	0.9766
15	1.0196	1.0005	1.0206	0.9948
20	1.0294	0.9963	1.0288	1.0036
25	1.0350	0.9935	1.0411	0.9913
30	1.0427	1.0341	1.0468	0.9805
33	1.0487	1.0089	1.0487	0.9585

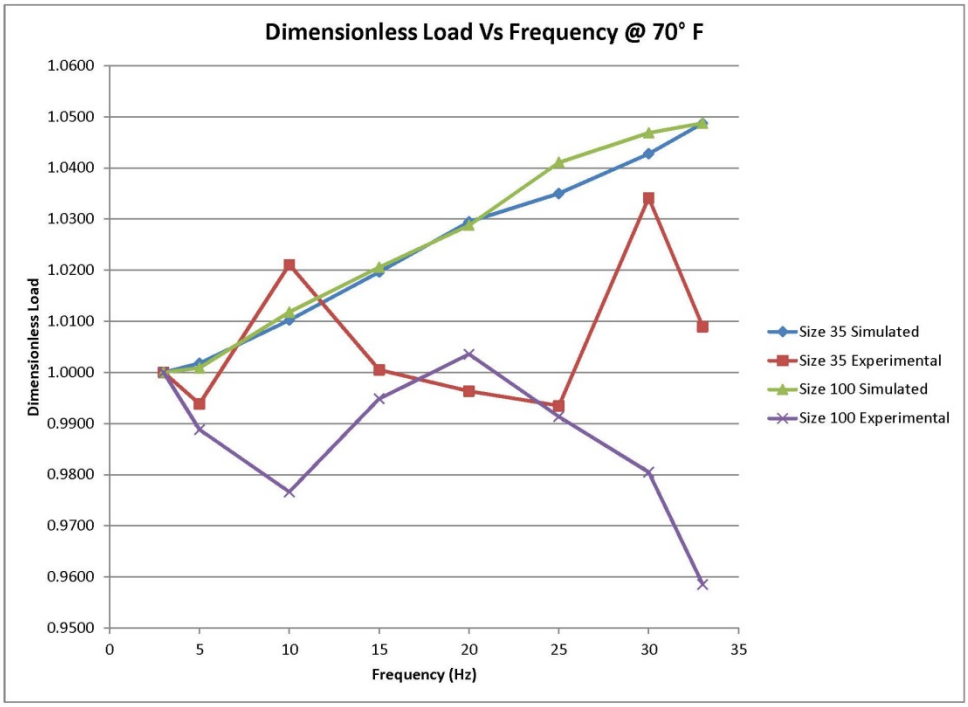

Figure 34 – Dimensionless Load Vs. Frequency

The reaction forces in the simulation are measured at nodes that are fixed relative to the moving piston assembly, and the load cell in the qualification tests was mounted on a moving actuator ram. Under load control, feedback from the load cell would cause the actuator to try to compensate for any inertial effects by increasing or decreasing load to the pre-determined test value. Actual values of load applied to the snubber are probably greater than the experimental test values. This would increase the stiffness of the experimental values and reduce their frequency dependence.

The two fluid parameters modeled include bulk modulus and shear viscosity of the hydraulic fluid. Experimentally, the bulk modulus of SF-1154 increases with pressure. Working pressures inside the hydraulic snubbers are higher than the simulated values, both due to the effect of the secondary reservoir adding fluid to the unloaded side each cycle, and increased loads cause by inertia. At higher frequencies, the pressure will be higher, stiffening the response. Also, altering the viscosity by orders of magnitude does not have much effect on the results of the dynamic simulations using the equation of state model. The hydrostatic response governs. Consideration was also given to the possibility that the increase in deflection as a function of frequency in the experimental data could be explained by the sinusoidal input approaching a natural frequency. Examining the experimental plot in Fig. 18, reduction in spring rate is approximately linear. If the snubber was approaching natural frequencies, values of deflection would increase exponentially with frequency.

A key difference between the dynamic simulations and the experimental test setup that has not yet been addressed is dead band, or lost motion. In the simulation,

there is no free movement due to manufacturing tolerances or clearances required for assembly. In the experimental test setup, the linear transducer was mounted to measure deflections between the cylinder and rod eye, and thus dead band was not measured. This does not mean it did not exist. This alters the input wave form, from a smooth sinusoid into the pumps controlling pressure in the actuator, to a sharp saw-toothed wave form seen at the connection of the snubber rod eye to the actuating bracket. The input wave form is now $Load(t) = A(t)P$, where P is the maximum test load and A(t) is a periodic coefficient that is a function of time. This wave form would look similar to the one seen in Fig. 35.

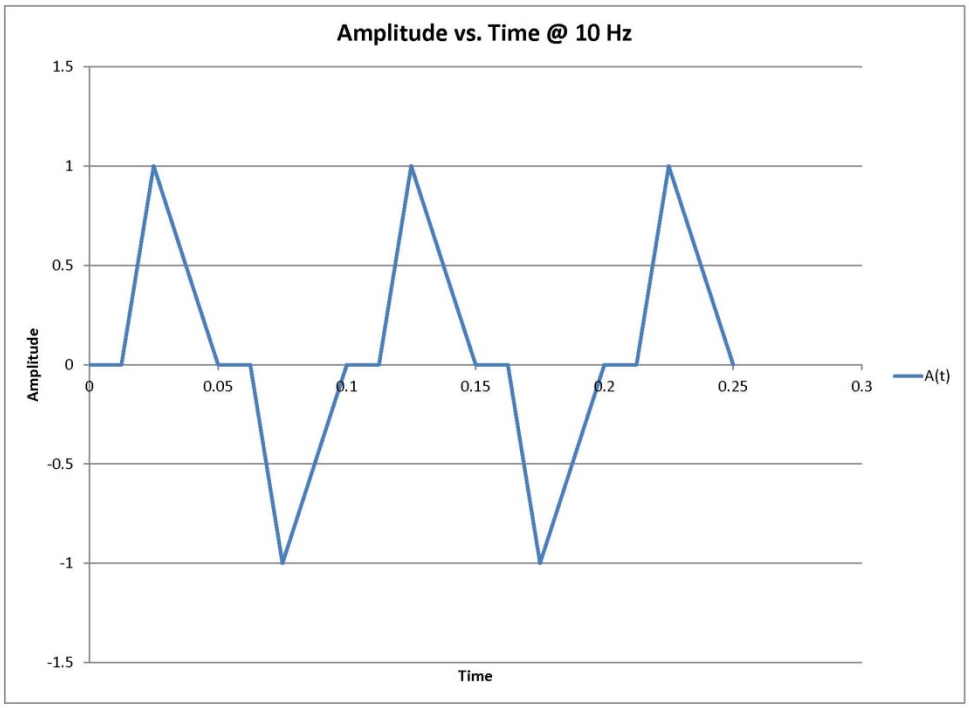

Figure 35 – Modified Waveform to Simulate Lost Motion

In a sinusoidal waveform, load increases from $t = 0$ to $t = \frac{T}{4}$, where T is the period. From $t = \frac{T}{4}$ to $t = \frac{3T}{4}$, load is decreasing to the minimum, and at t = T, load is zero. In Figure 35, from $t = 0$ to $t = \frac{T}{8}$, it as assume there is no load applied to the snubber due do lost motion. Deflections are on the magnitude of .04", and dead band is analytically determined to be .02". Thus, it is a reasonable assumption that ½ of the loading time interval is spent in free motion.

During the time when the snubber is unloaded due to deadband, pressure in the actuating cylinder is increasing. By the time the actuating ram makes contact with the snubber, the load applied is not zero, but a larger value. This impact load waveform now looks like Figure 36

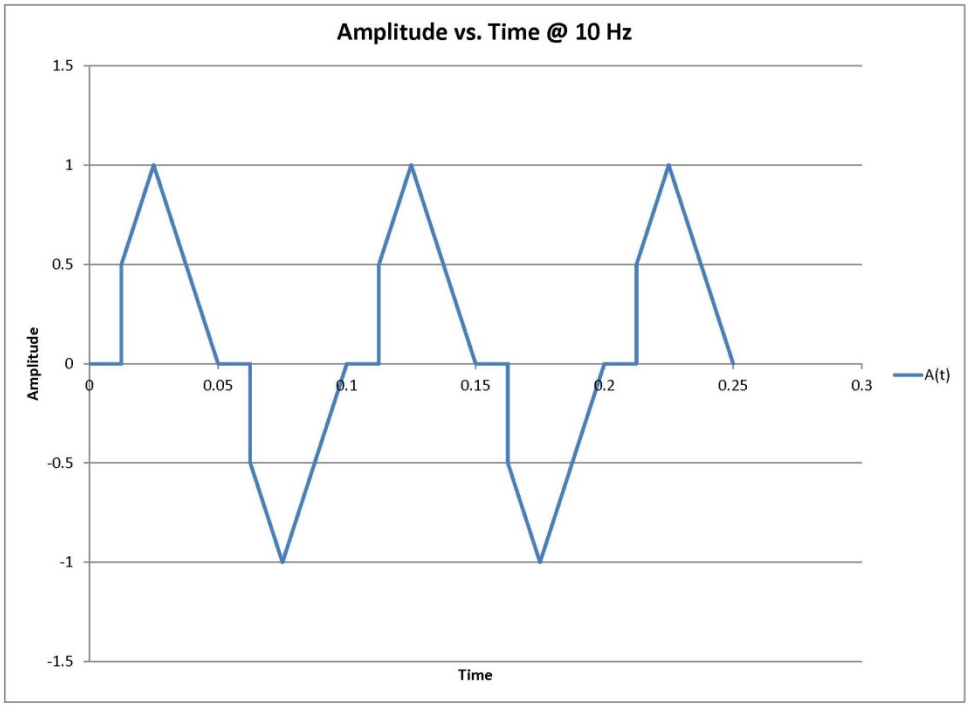

Figure 36 – Modified Waveform to Simulate Lost Motion and Impact Loading

In Fig. 36, it is assumed that the load applied at $t = \frac{T}{8}$ is ½ the maximum magnitude. This wave form can be applied to the dynamic model to test the effects of impact loading on dynamic response. The experimental value of the magnitude of the applied load at impact cannot be known from the data given, but an assumption will be made that it increases linearly with frequency, from 0 to .4. It will increase with frequency because of larger actuator accelerations at higher frequencies. Table 14 and Fig. 37 show simulated dimensionless spring rate plotted against actual dimensionless spring rate.

Table 14 - Dimensionless Spring Rate With Linearly Increasing Deadband Initial Load				
	Size 35		Size 100	
	Simulated	Experimental	Simulated	Experimental
3	1.0000	1.0000	1.0000	1.0000
5	0.9219	1.0382	0.9457	0.9170
10	0.7647	0.9965	0.6985	0.8795
15	0.5927	0.9338	0.8959	0.8195
20	0.7187	0.9028	0.7358	0.7597
25	0.7704	0.8175	0.4674	0.7210
30	0.7022	0.7603	0.3203	0.7334
33	0.6044	0.7148	0.5547	0.7307

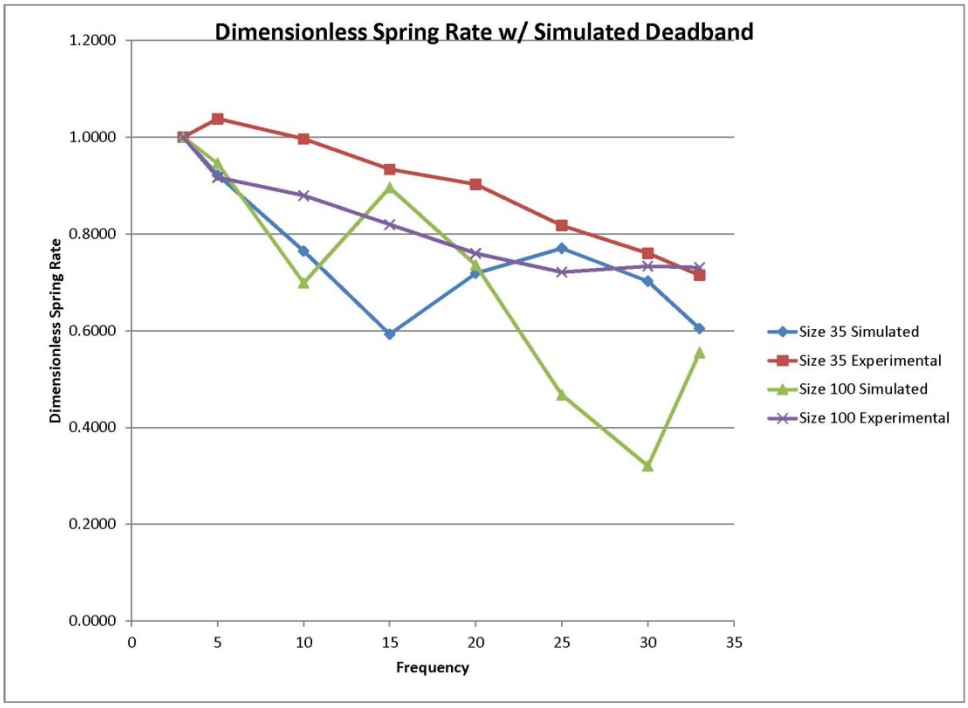

Figure 37 – Dimensionless Spring Rate w/ Simulated Deadband

The simulated dimensionless data trends downward, as does the actual dimensionless spring rate. While this looks promising, the simulated data is not predictable enough to say for certain that this is a trend or poor choice of modeling parameters. A drawback of using tie constraints to simulate the Newtonian fluid no-slip condition at media boundaries is that the internal fluid nodes can still drastically deform. There is no interaction or constraint defined for the internal fluid elements with respect to the metallic cavity surface. These elements are then allowed to deform beyond the tie constraints, locating some of their nodes "outside" the fluid cavity. This creates instabilities in the simulation. Adaptive meshing, a finer mesh, or a different element choice may fix these instabilities and give more uniform data.

For comparison, the acoustic medium fluid model was used to check the effects of simulated deadband on deflection. The interior nodes not subject to tie constraints of the cavity walls are subject to hydrostatic behavior only, and will not see the same excessive deformations due to shear forces that develop in the equation of state material model. Deadband was increased linearly with frequency, up to a maximum value of .4 of the initial load. The results are given in Table 15 and Figure 38. The simulation results for the Size 35 and 100 do show a more pronounced downward trend with this material model.

Table 15 - Dimensionless Spring Rate With Linearly Increasing Deadband Up to .4 Initial Load Utilizing the Acoustic Medium Fluid Model				
	Size 35		Size 100	
	Simulated	Experimental	Simulated	Experimental
3	1.0000	1.0000	1.0000	1.0000
5	0.9263	1.0383	0.9694	0.9169
10	0.9298	0.9966	0.9404	0.8795
15	0.8512	0.9338	0.9500	0.8195
20	0.9006	0.9029	0.9273	0.7597
25	0.7508	0.8176	0.9067	0.7210
30	0.5836	0.7603	0.8505	0.7333
33	0.5749	0.7148	0.7463	0.7307

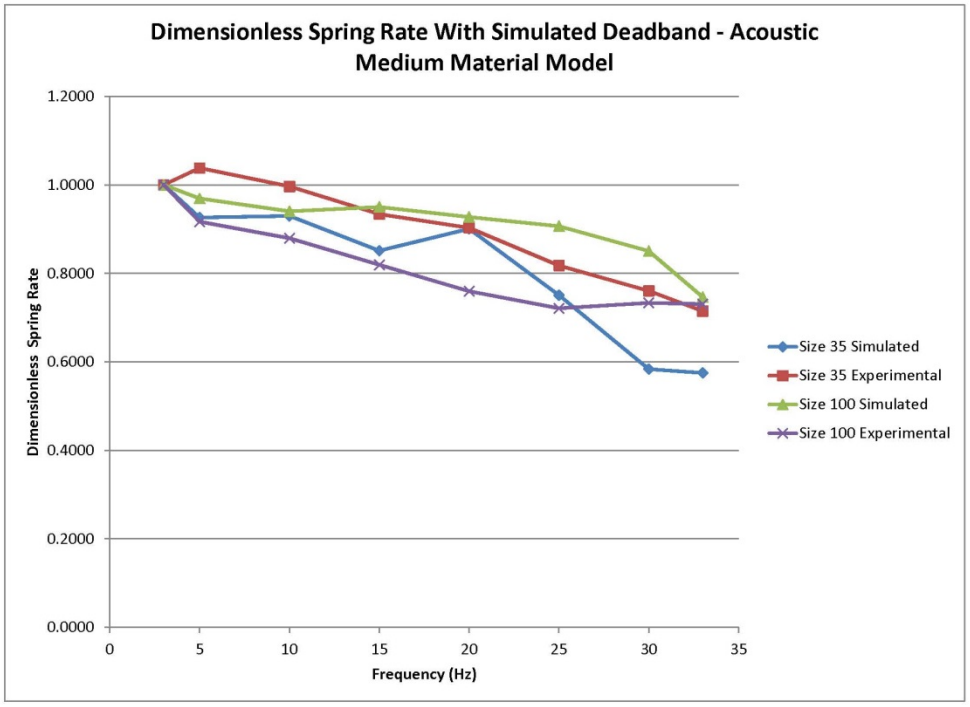

Figure 38 – Dimensionless Spring Rate with Simulated Deadband Utilizing the Acoustic Material Model

CHAPTER 6

Conclusion and Recommendations

Snubber dynamic spring rate is difficult to determine both experimentally and analytically. The controlling parameters are fluid bulk modulus, manufacturing tolerances, and assembly clearances. To reproduce the qualification test values on production units would require the exact duplication of all three parameters on each production model, which is impractical and cost prohibitive. An alternative might be dynamic testing of production units, and in fact some manufacturers do just that for smaller sizes. However, the experimentally determined value of spring rate on a production unit is only valid for that test and those test conditions. This includes parameters such as temperature, fluid bulk modulus, test load, pin clearances, piston position etc… Piping snubbers are installed in a myriad of applications and environmental conditions inside nuclear facilities, and the number of uncontrolled variables quickly invalidates any production dynamic test.

Large bore equipment snubbers are more heavily scrutinized during the design stage of the supported equipment. Their application is thoroughly studied and environmental variables are specified with a higher degree of certainty. On the manufacturer's side, large bore snubbers are quite often made for a specific application, so if the production unit is carefully studied all the dimensional parameters can be known. Fluid bulk modulus can still be problematic, as the fluid is usually replaced several times over a snubber's life cycle, but can be mitigated somewhat through quality control testing of each batch.

In conclusion, the FEA model showed only a 6% deviation from the static spring rate due to inertia of the piston assembly inside the cylinder. This is in contrast to the 30% deviation found in the experimental test values. However, the load control nature of the dynamic test understates the actual load seen by the snubber, decreasing the spring rate. It is also theorized that while the input of the hydraulic pumps into the actuating cylinder is sinusoidal, the actual waveform seen by the snubber is a combination of a step-function and sinusoid. This is a consequence of dead band, and as the initial load seen by the snubber during the loading intervals of each cycle increases, so too does deflection.

Further testing and study is required to say with certainty that an analytical method has been found for determining snubber spring rate with no testing. Specifically,

1) Conduct a similar analysis for the rest of the Fig. 3306 snubber product line. These cylinders are of a single piston rod configuration and have the same set of qualification test data available. There are 5 sizes of snubbers, which is a larger sample size than the scope of this study.
2) Performing further dynamic testing on the Size 35 and 100 will be cost prohibitive. If, after an analysis of the smaller sizes of Fig. 3306, the same result is shown, dynamic testing should be conducted on a smaller size. This time, instead of measuring load through a load cell in the load path, pressure transducers should be placed in the tension and compression fill ports. This way, the load seen by the snubber can be exactly measured independent of lost motion or inertia effects. Valuable insight will also be

gained into when exactly the check valves close each cycle, and what the working pressure of the snubber truly is.

3) Conduct dynamic testing at loads less than rated load on smaller sizes. In the simulations, applying the same simulated deadband to both sizes will not yield the same result. Testing at loads less than rated load could be conducted to find the correct input waveform for the simulations at those loads. It is possible that a trend can be found that can be found that can be applied to the full rated load of the snubber. For example, if deadband is accurately modeled against experimental tests conducted at 4% to 20% of rated load, perhaps the result can be applied to a simulation at 100% load.
4) Refine the finite element model to remove instabilities due to simulated dead band. The relationship between dead band and deflection of the snubber under an impact load can be better explored, and applied to the study of the smaller sizes.

Load controlled dynamic testing of hydraulic snubbers has always recorded the values of load with a load cell in the load path of a hydraulic actuator to the snubber, and has always been subject to the same limitations as discussed above. It may be that load controlled testing in this fashion does indeed show some frequency dependence that is overstated, and measuring loads through pressure transducers could show different results. Were this to happen, it would not invalidate a piping analysis done using the Anvil supplied stiffness as a minimum value as intended. In fact, if it could be demonstrated that frequency dependent effects are smaller than earlier reported,

one less parameter is required to accurately describe the snubber as a spring element on a piping system, and analytical models will become more accurate.

BIBLIOGRAPHY

[1] American Society of Mechanical Engineers Boiler and Pressure Vessel Code Section III Subsection NF, 2011 Edition, New York, New York

[2] Bush, Heasler, and Dodge, 1986, "Aging and Service Wear of Hydraulic and Mechanical Snubbers Used on Safety Related Piping and Components of Nuclear Power Plants", NUREG/CR-4279, Pacific Northwest Laboratory, Richland, WA

[3] Tagliamonte, M, Palmer, G.R., 1991 "Evolution of Snubber Testing", 1991 Snubber Users Group, Lake George, New York.

[4] Nitzel, Ware, and Page, 1992 "Technical Evaluation of Generic Issue 113: Dynamic Qualification and Testing of Large Bore Hydraulic Snubbers", NUREG/CR 5416, Idaho National Laboratory, Idaho Falls, Idaho

[5] American Society of Mechanical Engineers Operation and Maintenance of Nuclear Power Plants Subsection ISTD Preservice and Inservice Examination and Testing of Dynamic Restraints (Snubbers) in Light-Water Reactor Nuclear Power Plants, 2012 Edition

[6] Kumar, V, 1977 "A Parametric Study of the Effect of Locking Velocity and Bleed Rate Settings on the Dynamic Performance of ITT Grinnell Fig. 200 and Fig. 201 Hydraulic Snubbers", PHD 7579-S-1, Grinnell Corporation, Providence, RI

[7] "Design Response Spectra for Seismic Design of Nuclear Power Plants," Regulatory Guide 1.60 Revision 1, December 1973, US Atomic Energy Commission, Washington, DC

[8] Kornegay, John, C, 1976 “Test Procedure Preliminary Reduction of Data Snubber Environmental Test PHD-6507-1”, PHD-6507-1, Grinnell Corporation, Providence, RI.

[9]– American Society of Mechanical Engineers Qualification of Mechanical Equipment Code Subsection Qualification of Dynamic Restraints, 2007 Edition, New York, New York

[10] Information Notice 84-67 “Recent Snubber Inservice Testing with High Failure Rates”, August 1984, United States Nuclear Regulatory Commission Office of Inspection and Enforcement, Washington, DC.

[11] Fard, M.R., 2011 “Resolution of Generic Safety Issues Item A-13: Sunbber Operability Assurance (Rev. 2)”, NUREG-0933 Supplement 34, Division of Risk Analysis, United States Nuclear Regulatory Commission, Washington, DC.

[12] The Other Dynamic Loads and Load Combinations Task Group, 1984 “Report of the U.S. Nuclear Regulatory Commission Piping Review Committee Evaluation of Other Loads and Load Combinations”, NUREG-1061 Volume 4, United States Nuclear Regulatory Commission, Washington, D.C.

[13] Anderson, J, 1974 “Purchasing Specification for Shock Supressors” Document No. 21A3502 Rev. 2, General Electric Nuclear Energy Division, Atomic Power Equipment Department, San Jose, California.

[14] “Seismic Qualification of Electrical and Active Mechanical Equipment and Functional Qualification of Active Mechanical Equipment for Nuclear Power Plants”, Regulatory Guide 1.100 Revision 3, September 2009, United States Regulatory Commission Office of Nuclear Regulatory Research, Washington, DC

[15] Richards, R, 2009 “Figure 3306N/3307N Hydraulic Snubbers – Size 35 Summary of Functional Qualification Test Data”, PE 9851-6-06, Anvil EPS, North Kingstown, RI

[16] Richards, R, 2009 “Figure 3306N/3307N Hydraulic Snubbers – Size 100 Summary of Functional Qualification Test Data”, PE 9851-6-07, Anvil EPS, North Kingstown, RI

[17] American Society of Mechanical Engineers Boiler and Pressure Vessel Code Section II - Materials Part D, 2011 Edition, New York, New York.

[18] “Abaqus 6.13 Online Documentation”, Generated Tuesday, April 2, 1013 at 15:33:39, Dassault Systemes, 2013

[19] Eisenhut, Darrell, “Technical Specification Revisions For Snubber Surveillance”, Generic Letter 80-99, September 1980. United States Nuclear Regulatory Commission Division of Licensing, Washington, DC.

[20] Eisenhut, Darrell, “Technical Specification For Snubbers”, Generic Letter 84-13, May 1984. United States Nuclear Regulatory Commission Division of Licensing, Washington, DC.

[21] Richards, R, 2007 “Functional Qualification Test Procedure Fig. 3306N Hydraulic Snubbers to Meet General Electric Requirements”, PE 9851-3, Anvil EPS, North Kingstown, RI